UC San Diego
UC San Diego Electronic Theses and Dissertations

Title
Anomalous radial transport in tokamak edge plasma

Permalink
https://escholarship.org/uc/item/3zm828hb

Author
Bodi, Vasudeva Raghavendra Kowsik

Publication Date
2010

Peer reviewed|Thesis/dissertation

UNIVERSITY OF CALIFORNIA, SAN DIEGO

Anomalous radial transport in tokamak edge plasma

A dissertation submitted in partial satisfaction of the
requirements for the degree
Doctor of Philosophy

in

Engineering Sciences (Aerospace Engineering)

by

Vasudeva Raghavendra Kowsik Bodi

Committee in charge:

    Professor Sergei Krasheninnikov, Chair
    Professor Farhat Beg
    Professor Patrick Diamond
    Professor Asoka Mendis
    Professor Sutanu Sarkar

2010

The dissertation of Vasudeva Raghavendra Kowsik Bodi is approved, and it is acceptable in quality and form for publication on microfilm and electronically:

_____

_____

_____

_____

_____
Chair

University of California, San Diego

2010

TABLE OF CONTENTS

LIST OF FIGURES

LIST OF TABLES

ACKNOWLEDGEMENTS

Chapters 5& 6 contain material in preparation to be published as "Anomalous radial transport model for kinetic codes", K. Bodi, R. H. Cohen, S. I. Krasheninnikov, T. D. Rognlien and X. Q. Xu. The dissertation author is the primary author of this publication. The text of chapter 6 contains material in communication to be published as "TEMPEST simulations of the plasma transport in a single-null tokamak geometry", X. Q. Xu, K. Bodi, R. H. Cohen, S. Krasheninnikov and T. D. Rognlien, Nuclear Fusion. The dissertation author is a contributing author of this publication.

VITA

2002	B. Tech. in Aerospace Engieering Indian Institute of Technology Madras, Chennai, India
2005	M. Sc. (Engg.) in Aerospace Engineering Indian Institute of Science, Bangalore, India
2005-2009	Graduate Research Assistant Department of Mechanical and Aerospace Engineering University of California, San Diego
2007	Teaching Assistant CENG101A: Introductory Fluid Mechanics Department of Mechanical and Aerospace Engineering University of California, San Diego
2009	Teaching Assistant MAE118A: Introduction to Energy Systems Department of Mechanical and Aerospace Engineering University of California, San Diego
2010	Ph. D. in Engineering Sciences (Aerospace Engineering), University of California, San Diego

PUBLICATIONS

K. Bodi, R. H. Cohen, S. I. Krasheninnikov, T. D. Rognlien and X. Q. Xu, "Anomalous radial transport model for kinetic codes", In Preparation.

X. Q. Xu, K. Bodi, R. H. Cohen, S. Krasheninnikov and T. D. Rognlien, "TEMPEST simulations of the plasma transport in a single-null tokamak geometry", *Nuclear Fusion*, In Communication.

K. Bodi, A. I. Smolyakov and S. I. Krasheninnikov, "On blob generation mechanisms in tokamak edge plasma", *Journal of Nuclear Materials*, 390-391: 359, 2009

K. Bodi, S. I. Krasheninnikov and A. I. Smolyakov, "Blob dynamics in an inhomogeneous plasma", *Physics of Plasmas*, **15**(10): 102304, 2008.

K. Bodi, S. I. Krasheninnikov, and A. I. Smolyakov, "On the mechanisms of generation of meso-scale convective structures in tokamak edge plasma", *Contributions to Plasma Physics*, **48**(1-3): 63, 2008.

ABSTRACT OF THE DISSERTATION

Anomalous radial transport in tokamak edge plasma

by

Vasudeva Raghavendra Kowsik Bodi

Doctor of Philosophy in Engineering Sciences (Aerospace Engineering)

University of California San Diego, 2010

Professor Sergei Krasheninnikov, Chair

Energy from nuclear fusion of Hydrogen isotopes is a possible alternative to fossil fuels. For this to be of practical utility, confinement of Hydrogen in a plasma state for a minimum duration is necessary. Since confinement is strongly affected by radial transport processes, understanding the observed modes of radial transport in confined plasma is of vital importance for progress towards fusion energy. The present dissertation is aimed at studying radial(cross-field) transport in the tokamak edge plasma.

The present thesis is divided into three parts:

- In the first part, we present a model of generation of intermittent convective meso-scale structures (blobs) based on the synergy of the interchange drive and nonlinear effects associated with drift–wave turbulence.

- In the second part, we attempt to explain the preferential propagation of blobs radially outward as a consequence of the radially decreasing density of a confined plasma.

- In the third part, we present a model for simulating anomalous radial transport in kinetic codes for tokamak edge plasma.

Chapter 1

Introduction

1.1 Background

Energy from nuclear fusion of Hydrogen isotopes is a possible alternative to fossil fuels. The abundance of Hydrogen in nature (in the form of water) and the large amount of energy released in a fusion reaction per unit fuel mass make this an attractive alternative in comparison with other sources of energy.

For a nuclear fusion based power plant to be of practical utility, one should achieve a steady–state energy output from a spatially confined fuel. A quantitative criterion, called Lawson's criterion, to verify the practicability of the concept can be defined as the condition that the energy output from the fusion reactor exceeds the energy required to make it operational. In terms of plasma density, n, and the duration of confinement, τ_E, Lawson's criterion can be written as,

$$n\tau_E \geq 2 \cdot 10^{20} \text{m}^{-3}\text{s}$$

A significant hurdle towards arriving at the working design of any powerplant has been the availability of suitable materials that can withstand the material stresses involved in the operation of the powerplant. In order to achieve optimum power output, the temperature of fusion–plasmas should be of the order of $2 \cdot 10^8$ K. Plasma at such a high temperature can corrode any material that it comes into contact with, and hence an alternative confinement mechanism is required.

The present work concerns the spatial confinement of high temperature plasmas by the application of magnetic fields. In particular we are interested in plasma confined using a combination of toroidal and poloidal magnetic fields. Such a confinement device, resulting in a plasma confined in the shape of a torus, is known as a *tokamak*. A detailed introduction to tokamak plasma can be found in the books by Kadomtsev [1] and Wesson [2]. In the present work we are interested in the effect of anomalous transport processes on the confinement of tokamak plasma. Since confinement is strongly affected by transport processes in the plasma, understanding the observed modes of transport in confined plasma is of vital importance for progress towards fusion energy.

1.2   Transport in tokamak plasma

Classical transport in tokamak plasma is determined by Coulomb collisions, and hence can be expressed as diffusive transport, with the transport coefficient

$$D \sim \Delta^2 \nu$$

where ν is the collision frequency and Δ is the collisional step–size. In a uniform magnetic field the charged particle gyro–radius is the collisional step–size. In a tokamak, since the magnetic field is non–uniform, charged particle drifts result in the motion of particles across the flux–surfaces. The width of the particle drift–orbits across the flux–surfaces forms the collisional step–size [3]. This description is known as neoclassical theory, in contrast to the classical theory that describes collisional transport in uniform magnetic field. A review of classical and neoclassical transport theory for tokamak plasma can be found in Ref. [4].

Unfortunately transport predicted by the classical and neoclassical theories can not fully explain that observed in experiment. The difference between the observed transport, and that predicted by collisional theories, is known as *anomalous* transport and is believed to be primarily due to turbulent plasma processes. Unlike classical transport which is purely diffusive, anomalous transport is believed to be contain a convective component [5]. Based on experimental observations

of tokamak edge plasma, it is now believed that anomalous radial transport consists of intermittent convecting structures, that are elongated along the fieldlines, whose extent in the perpendicular plane (to the fieldlines) is larger than the gyroradii (*micro*scales) but smaller than the confinement dimensions (*macro*scales) and thus, referred to as belonging to the *meso*scales. These structures are referred to as blobs, since their density differs from that of the surrounding plasma. The mechanism of propogation of blobs in tokamak edge was first explained in [6]. Curvature and ∇B drifts on the outer side of the torus act as effective gravity,
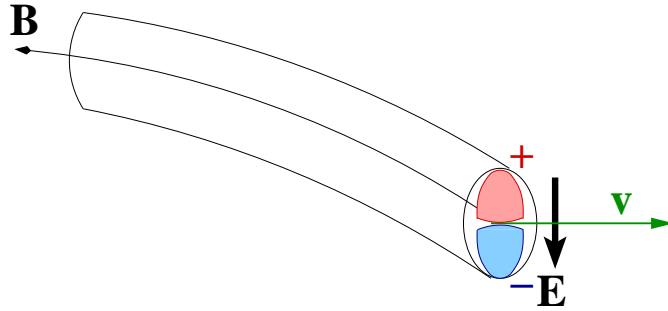
Figure 1.1: Illustration of the mechanism of blob propogation on the outer side of tokamak.

and result in plasma polarization. The resulting vertical electric field causes an $E \times B$ drift which is radially outward towards the chamber walls. This process is illustrated in Fig. 1.1. The mechanism of propogation of such coherent structures in the scrape-off layer has been the studied by analytical and numerical methods ([7] for example), a review of the current understanding of blobby transport can be found in [8].

In chapters 2 & 3 we concentrate on the mechanism of generation of blobs in tokamak edge plasma using analytical and numerical methods. In chapter 4 we study the effect of the edge plasma density gradients on the propogation of blobs using numerical simulations. In chapter 5 we introduce the kinetic code TEMPEST [9] for simulating edge plasma transport, and present a particle and energy conserving Krook model for computing the effect of collisions. In chapter 6 we present a model for anomalous radial transport computations in kinetic transport codes for tokamak edge plasma.

1.3   Numerical simulations of tokamak plasma

In the absence of sufficient information for analytical models, numerical simulations are an alternative approach for verifying our understanding, and applying the derived insights towards estimating effects of any proposed modifications before their implementation. Numerical simulations are also needed to extrapolate the understanding derived from the existing devices towards the design and operation of larger devices (like ITER).

Efforts are in progress at many groups towards developing computation tools that can help understand the experimental observations [10]. A necessary prerequisite for any such tool is that it must first demonstrate the physical phenomena that have already been satisfactorily explained by analytical theories. The computational tools can then be tested by progressively tackling increasingly complex phenomena observed in plasma confinement devices. Complex phenomena that are yet to be fully understood can then be tackled using such computational tools.

In chapters 3 & 4 we use numerical simulations to verify the analytical understanding of the mechanism of generation and propagation of blobs. In these chapters we are interested in the closed field–line region of the tokamak edge plasma. We describe the plasma in this region using fluid equations. We further reduce the computational expense by considering a small section of the poloidal plane. This allows us the efficiency of computation required for simulating plasma turbulence.

While the fluid description is reasonable in the closed field–line region, its applicability in the open field–line region in the edge scrape-off layer (SOL) is debatable. This uncertainty in its applicability is primarily due to the fact that the field–line connection length is comparable to the particle mean free path in the hotter parts of the scrape–off layer. An additional source of complexity in this region is that, since the gradients are sharp in this region in H–mode plasma, the gradient length–scales in the parallel direction can be comparable to the particle mean free paths. Hence, numerical simulations for tokamak edge plasma must solve the kinetic equations. Chapter 5 contains a brief description of the kinetic

code TEMPEST, and the formulation & implementation of a particle and energy conserving Krook collision model to include the effects of thermal relaxation in the code. Chapter 6 concerns the formulation of a model for anomalous transport, and its implementation in the kinetic code TEMPEST.

1.4   Dissertation outline

The present thesis is divided into three parts:

1.4.1   Chapters 2 & 3: Generation mechanisms of blobs in tokamak edge plasmas

Radial transport at the edge of magnetic confinement devices (such as a tokamak) has been found to be often dominated by intermittent convective-like transport in the form of meso-scale coherent structures that are extended along the magnetic field lines. Such filament-like structures can propagate in a ballistic way toward the wall, for the distance of ten centimeters or more, and can strongly enhance both plasma energy and particle transport and plasma-wall interactions. The apparent examples of such meso-scale structures in the edge and the SOL plasmas are ELMs and blobs, and pellet clouds in the core of fusion devices.

In this work we show that the interplay of the interchange drive and nonlinear effects associated with drift wave turbulence (which is rather strong at the edge in L-mode) can lead to the blob formation. In particular, we discuss the possible mechanism of blob generation due to synergetic effects of a) the interchange drive, b) turbulent Reynolds stress, and c) local plasma perturbations associated with inverse cascade of the drift-wave turbulence. We note that recent experimental observations qualitatively agree with a physical picture of blob generation outlined in this paper.

This work has been published as

- K. Bodi, S. I. Krasheninnikov, and A. I. Smolyakov, *On the mechanisms of generation of meso-scale convective structures in tokamak edge plasma*, Contributions to Plasma Physics, 48(1-3):6367, 2008. Proceedings of the 11th International Workshop on Plasma Edge Theory in Fusion Devices.

- K. Bodi, A.I. Smolyakov, and S.I. Krasheninnikov, *On blob generation mechanisms in tokamak edge plasma*, Journal of Nuclear Materials, 390-391:359 363, 2009. Proceedings of the 18th International Conference on Plasma-Surface Interactions in Controlled Fusion Device.

1.4.2 Chapter 4: Blob propagation in non-homogeneous plasma

In this work we look at the convective blob propagation in the Scrape-Off-Layer and/or limiter shadow region with emphasis on the effect of a gradient in the equilibrium plasma density. We consider the effect of the gradient of equilibrium plasma density beyond the Boussinesq approximation. We show that the vorticity modification due to the plasma density gradient leads to the acceleration for the blobs propagating into the region of lower density and deceleration for the blobs propagating toward the regions of higher density. Analytical estimates are corroborated by direct numerical simulations.

This work has been published as:

- K. Bodi, S. I. Krasheninnikov, and A. I. Smolyakov. Blob dynamics in an inhomogeneous plasma. Physics of Plasmas, 15(10):102304, 2008.

1.4.3 Chapters 5 & 6: Modeling & simulation of anomalous radial transport in kinetic codes for edge plasma

Modeling of anomalous (turbulence-driven) radial transport in controlled fusion plasmas is necessary for long-time transport simulations. Here the focus is

continuum kinetic edge codes such as the (2-D, 2-V) transport version of TEM-PEST, NEO, and the code being developed by the Edge Simulation Laboratory, but the model also has wider application. We present an anomalous diagonal transport matrix model with velocity-dependent convection and diffusion coefficients that allows contact with typical fluid transport models (e.g., UEDGE). We also present a particle and energy conserving Krook collision model that can be used to compute collisional transport due to ion drift orbits.

Chapter 2

Mechanism of blob generation in tokamak edge

2.1 Introduction

Cross-field plasma transport in both L- and H-mode plasmas is characterized by intermittent radial convection of filamentary structures elongated along the magnetic field ([11–17]). Such coherent meso-scale structures have been called blobs and ELM filaments in L- and H-mode regimes respectively. While peeling-ballooning instabilities and their subsequent nonlinear saturation have been cited as the mechanism of ELM generation [18–20], plasma polarization (due to magnetic field curvature) has been suggested ([6, 8]) to be an underlying mechanism for the formation and convection of blobs. It has also been recently proposed that nonlinear plasma polarization due to Reynolds stresses associated with small-scale drift-wave turbulence can be an important factor in the formation of electromagnetic meso-scale structures i.e., blobs [21].

Generically, the process of formation of meso-scale structures as a result of modulational instability of drift waves has been a subject of intensive studies for a long time [22–26]. It is widely recognized now that such structures, in particular zonal flows, play a critical role in regulation and saturation of drift wave turbulence and transport ([27–33]). Our analysis of turbulent blob generation in [21] was based

on the application of the wave kinetic equation approach. Here we consider the same process of blob generation by using the four-wave interaction approach. We also discuss the effects of equilibrium plasma density variation on the propagation of seeded blobs. In Section 2.2 we present the system of equations and review the results of [21]. In Section 2.3 we consider the generation of blobs through the modulational instability of drift waves based on the four-wave interactions.

2.2 Governing equations

We use a system of reduced fluid equations (the notation is standard) that can be obtained from standard fluid equations by expansion in $1/B$ parameter [34]. In the low frequency, $\omega < \omega_{c_i}$, and long wavelength, $k_\perp^2 \rho_i^2 < 1$, approximations, for low plasma pressure $\vec{\nabla} \times \vec{B} - 0$, the electron continuity equation reduces to a simple form:

$$\left(\frac{\partial}{\partial t} + \vec{V}_E \cdot \vec{\nabla} \right) n - 2n \left(\vec{V}_E + \vec{V}_{pe} \right) \cdot \vec{\nabla} \ln B - \frac{1}{e} \nabla_\| J = 0 \tag{2.1}$$

where $\vec{V}_E = \left(\hat{e}_z \times \vec{\nabla} \phi \right) / B$, $\vec{V}_{pe} = -\left(\hat{e}_z \times \vec{\nabla} p_e \right) / (enB)$, and $\hat{e}_z = \vec{b}$ is the direction of the local magnetic field. The nonlinear parallel gradient operator ($\nabla_\|$) is defined as

$$\nabla_\| (\dots) = \left(\frac{\partial}{\partial z} + \frac{1}{B} \vec{B} \cdot \vec{\nabla} \right) (\dots) = \frac{\partial}{\partial z} (\dots) - \frac{1}{B_0} \hat{e}_z \cdot \left[\vec{\nabla} A \times \vec{\nabla} (\dots) \right] \tag{2.2}$$

Here A is the parallel component of the vector potential that describes magnetic perturbations $\vec{B} = -\hat{e}_z \times \vec{\nabla} A$. The parallel component of the electric current is $J = -\left(1/\mu_0 \right) \nabla_\perp^2 A$. In the regime of $\omega < k_\| \mathrm{v}_{T_e}$, which is assumed in our work, Ohm's law is

$$\frac{1}{c} \frac{\partial A}{\partial t} + \nabla_\| \left(\phi - \frac{T_e}{e} \ln n \right) = 0 \tag{2.3}$$

For finite T_i plasma, inertial polarization drift and the ion drift due to gyroviscosity contribute to the Reynolds stress, which is responsible for generation of large–scale structures; hence these terms are retained in the present analysis. Taking into

account the gyroviscous cancellation (e.g. see [34] and [35–37]), ion continuity equation is

$$\left(\frac{\partial}{\partial t} + \vec{V}_E \cdot \vec{\nabla}\right) n - 2n \left(\vec{V}_E + \vec{V}_{pe}\right) \cdot \vec{\nabla} \ln B - n_0 \rho_i^2 \vec{\nabla}_\perp \cdot \left[\frac{d_0}{dt}\left(\frac{e\vec{\nabla}_\perp \phi}{T_i} + \frac{\vec{\nabla}_\perp p_i}{p_i}\right)\right] = 0$$

(2.4)

where, $\vec{V}_{pi} = \left(\hat{e}_z \times \vec{\nabla} p_i\right)/(enB)$,

$$\frac{d_0}{dt}(\dots) = \left(\frac{\partial}{\partial t} + \left[\frac{c}{B_0}\hat{b} \times \vec{\nabla}\phi\right] \cdot \vec{\nabla}\right)(\dots) = \frac{\partial}{\partial t}(\dots) + \frac{c}{B_0}\hat{b} \cdot \left[\vec{\nabla}\phi \times \vec{\nabla}(\dots)\right]$$

Quasineutrality equation is,

$$-\nabla_\parallel J + \frac{2}{B}\left[\hat{e}_z \times \vec{\nabla}(p_e + p_i)\right] \cdot \vec{\nabla}\ln B + en_0\rho_i^2 \vec{\nabla}_\perp \cdot \left[\frac{d_0}{dt}\left(\frac{e\vec{\nabla}_\perp \phi}{T_i} + \frac{\vec{\nabla}_\perp p_i}{p_i}\right)\right] = 0$$

(2.5)

2.2.1 Separation of Scales

In the following analysis, all perturbed quantities are represented as a sum of large-scale and small-scale components, $X = X_k + X_q$, $q < k$, where k and q are the small and large-scale wave-numbers respectively. An analogous separation of scales is assumed in the time domain, $\Omega_q < \omega_k$: ω_k are the eigen-frequencies of small-scale fluctuations, $X_k \sim \exp(-i\omega_k t)$ and Ω_q are the large-scale mode frequencies, $X_q \sim \exp(-i\Omega_q t)$. The latter are affected by nonlinear effects and can deviate significantly from the linear eigenvalues.

2.2.2 Inverse cascade and ballooning instability of meso-scale structures

In [21], blob generation was explained as a synergy of the interchange drive and nonlinear effects associated with drift wave turbulence. The Reynolds stress was obtained using the wave kinetic equations. Based on the resulting dispersion relation, an instability criterion was derived for the ensemble averaged magnitude

$(\langle\phi\rangle)$ and length-scales $(\langle k_x\rangle)$ of the fluctuations for the destabilizing turbulent stresses to overcome the Alfven stabilization (for $\beta = c_s^2/v_A^2$)

$$\rho_s\langle k_x\rangle\frac{e\langle\phi\rangle}{T} > \frac{1}{q_s R q_y \sqrt{\beta}} \tag{2.6}$$

where q_s is the safety factor. For the large-scale modes, an instability criterion was derived to explain the length-scales, Δ, of the meso-scale structures. A simple, order of magnitude estimate was obtained for large plasma fluctuations by taking $q_y\Delta \sim 1$, and neglecting the destabilizing effect of turbulent stresses in the instability criterion

$$\frac{c_s^2}{R\Delta} - \frac{c_s^2\rho_s^2}{\Delta^4} > \frac{V_A^2}{q_s^2 R^2} \tag{2.7}$$

The competition of the first and second terms defines the characteristic size of meso-scale structure for which the left hand side is maximal:

$$\Delta_m \approx \left(\rho_s^2 R\right)^{1/3} \tag{2.8}$$

(we assume that $\Delta_m < L_n$, where L_n is the density scale length). Then the instability within this flux tube occurs for relatively high beta at the edge of plasma

$$\beta > q^{-2}\left(\rho_s/R\right)^{2/3} \tag{2.9}$$

2.3 Blob generation via modulational instability of drift waves

In this section, we follow the approach of four-wave modulational interaction to study blob generation. We proceed from the above-described separation of scales, and for the primary fluctuations, we consider simple drift-wave type fluctuations assuming that primary modes are electrostatic and that the condition $\omega \leq k_{\parallel}v_{T_e}$ is satisfied. In this case, the electron density response is,

$$n_k = \frac{e\phi_k}{T_e}n_0$$

The ion response takes into account the equilibrium gradients of density and ion temperature (which are assumed to be small enough to avoid ITG instability). In

the lowest order, neglecting the effects of dispersion and the gradient of the equilibrium magnetic field, we obtain the simple electron drift-wave primary fluctuations

$$\omega = \omega_{*k} = -k_y \frac{cT_e}{eB_0} \frac{1}{n_0} \frac{\mathrm{d}n_0}{\mathrm{d}x} \equiv k_y \mathrm{v}_*$$

where, $\mathrm{v}_* = -\left(cT_e/eB_0\right) n_0'/n_0$. Nonlinear interaction of these primary fluctuations with large-scale components leads to the excitation of the sidebands of the perturbed quantities, which can be obtained from the respective governing equations. We assume that the ion temperature sidebands follow the simple relation

$$\frac{T_{\pm k+q}}{T_{0_i}} = \left(\frac{\partial \ln T_{0_i}}{\partial \ln n_0}\right) \frac{e\phi_{\pm k+q}}{T_e} \equiv \eta_i \frac{e\phi_{\pm k+q}}{T_e}$$

where, we have defined η_i as: $\eta_i = \partial \ln T_{0_i}/\partial \ln n_0$. This neglects the nonlinear generation of temperature sideband via convection. Since the small-scale fluctuations are electrostatic ($A_k = 0$), Ohms law can be written as

$$-i\frac{1}{c}\left(\Omega - q\mathrm{v}_*\right) A_{k+q} + i\frac{T_e}{e}\left(q_z + k_z\right)\left(\frac{e\phi_{k+q}}{T_e} - \frac{n_{k+q}}{n_0}\right) = 0 \qquad (2.10)$$

Corrections due to A_{k+q}, are small (of the dispersive order, e.g. $k_\perp^2 \rho_i^2$), and are neglected here. As a result, we have no direct generation of sidebands of the vector potential in the Ohms law and the sidebands of primary fluctuations remain electrostatic

$$\frac{e\phi_{k+q}}{T_e} = \frac{n_{k+q}}{n_0}$$

Neglecting the dispersive corrections, thus leading to $A_{\pm k+q} = 0$, the large-scale component of the parallel momentum balance remains linear

$$\frac{1}{c}\frac{\partial A_q}{\partial t} + \frac{\partial}{\partial z}\left(\phi_q - \frac{T_e}{e}\frac{\tilde{n}_q}{n_0}\right) + \frac{1}{c}\frac{cT_e}{eB_0}\frac{1}{n_0}\hat{e}_z \cdot \left(\vec{\nabla} A_q \times \vec{\nabla} n_0\right) = 0 \qquad (2.11)$$

For $\Omega < q_z \mathrm{v}_{T_e}$, electron and ion temperature fluctuations are determined by

$$\nabla_\parallel T_e = 0$$

$$\frac{\partial T_{i_q}}{\partial t} + \vec{\mathrm{v}}_{E_q} \cdot \vec{\nabla} T_{0_i} = 0 \qquad (2.12)$$

Neglecting the magnetic gradient drift and parallel current terms (of the dispersive order) in the electron continuity equation, we have

$$\frac{n_q}{n_0} = \frac{q\mathrm{v}_*}{\Omega}\frac{e\phi_q}{T_e} \qquad (2.13)$$

Denoting the contribution of Reynolds stress as $\mathcal{R}_1$, the quasineutrality equation is

$$\Omega_{D_i}\left(\frac{n_q}{n_0}+\frac{T_{i_q}}{T_{0_i}}\right)-\Omega_{D_e}\left(\frac{n_q}{n_0}+\frac{T_{e_q}}{T_{0_e}}\right)$$
$$-\Omega q_\perp^2\rho_i^2\left(\frac{n_q}{n_0}+\frac{T_{i_q}}{T_{0_i}}+\frac{\rho_s^2}{\rho_i^2}\frac{e\phi_q}{T_e}\right)+\frac{c}{4\pi en_0}q_z q_\perp^2 A_q+i\rho_i^2\mathcal{R}_1=0$$

$$(2.14)$$

where $\Omega_{D_{i,e}}=q_y\mathrm{v}_{D_{i,e}}$, $\mathrm{v}_{D_{i,e}}=\pm cT_{i,e}/eB_0\partial\ln B/\partial x$, $\tau=T_{0_i}/T_{0_e}$, $\rho_s^2=T_e/m_i\omega_{c_i}^2$, $\rho_i^2=\tau\rho_s^2$. Linearizing Eq. 2.12 for the electron and ion temperature fluctuations, and Eq. 2.13 for density fluctuations, neglecting dispersion in the large-scale components, we obtain the lowest order expressions for the Reynolds stress, leading to the final dispersion relation

$$\Omega^2+\Omega\Omega_*\tau\left(1+\eta_i\right)-\frac{\Omega_{D_i}\Omega_*}{q_\perp^2\rho_s^2}\left[1+\eta_i+\tau^{-1}\left(1+\eta_e\right)\right]-q_z^2\mathrm{v}_A^2$$
$$=-2\left(\frac{c}{B_0}\right)^2\left|\hat{e}_z\cdot\left(\vec{k}\times\vec{q}\right)\right|^2|\phi_k|^2\left(1+\tau^{-1}+\eta_i\right)\qquad(2.15)$$

Here, the second term describes the drift stabilization due to finite ion temperature, the third term is the interchange drive, and the fourth term describes the Alfven stabilization. The term on the right-hand side is the Reynolds stress drive that takes into account the diamagnetic contributions due to finite ion temperature. Eq. 2.15 is consistent with results of the previous analysis following the wave kinetic approach [21]. Note that the growth rate of this electromagnetic instability is a factor $q\rho_s$ larger than for electrostatic modes with a finite q_y.

2.4 Summary

We can see, from equations 2.7 – 2.9, that there is a length–scale limit for the stability of a meso–scale structure. Structures having a perpendicular length–scale larger than Δ_m are thus propelled away from the remaining confined plasma, and appear to us as "blob"s. In the following chapter, we describe numerical investigations to verify the explanation for blob generation that has been described in the present section.

Chapter 2 is, in its entirety, a reprint of the material published in "On blob generation mechanisms in tokamak edge plasma", K. Bodi, A.I. Smolyakov, and S.I. Krasheninnikov, Journal of Nuclear Materials, 390-391:359 (2009). The dissertation author was the primary author of this publication.

Chapter 3

Numerical simulations

In the present chapter, we present the computational investigation of the generation of blobs as a result of the interplay between drift-wave turbulence, interchange drive and field-line stabilization. In Sec. 3.1 we present the governing equations for edge plasma that describe the physical processes that are of interest. In Sec. 3.2, we describe the computational method used in the simulations. The initial equilibrium state and the results of the simulations are presented in sections 3.3 and 3.4 respectively.

3.1 Governing equations

We consider a tokamak of major radius R_0 and minor radius a, and introduce local coordiantes, x, y and z along the radial, poloidal and toroidal directions, as shown in Fig. 3.1. We start with the equations derived in the standard aspect ratio expansion, $\varepsilon = a/R \ll 1$, [38]. We consider the edge region of plasma on the outerside of the tokamak where the magnetic field can be expressed by a vector potential using

$$\vec{B} = B\hat{b} = B_z \hat{e}_z + \vec{B}_\perp = B_z \hat{e}_z - \hat{e}_z \times \vec{\nabla} A_z \tag{3.1}$$

where $B_z = B_0 \left(1 - x/R\right)$ is the component of the static magnetic field along the toroidal direction, and $B_\perp$ is generated by the plasma current j_z:

$$j_z = -\frac{c}{4\pi} \nabla_\perp^2 A_z \tag{3.2}$$
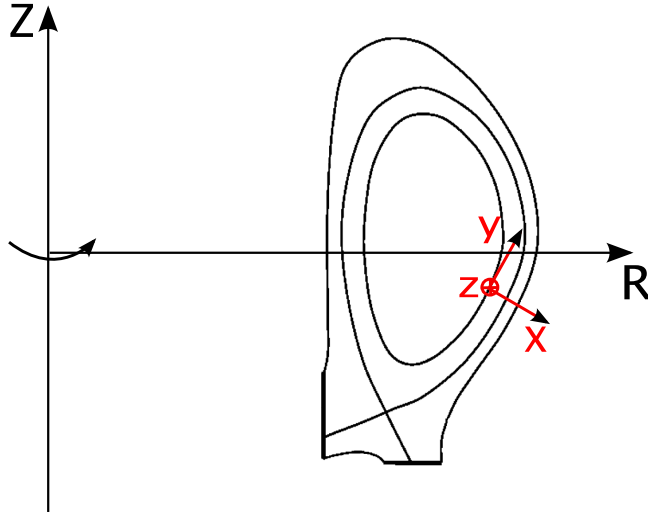
Figure 3.1: Schematic of the local coordinates.

The vorticity equation

$$\frac{cMn_0}{B^2}\left(\frac{\partial}{\partial t} + \vec{V} \cdot \vec{\nabla}\right)\nabla^2\phi + \frac{T_e}{BR}\frac{\partial n}{\partial y} = \frac{1}{c}\left(\hat{b} \cdot \vec{\nabla}\right)j_z \tag{3.3}$$

is derived using the Boussinesque approximation. Here M is the mass of the ions, c is the velocity of light, ϕ is the electrostatic potential, $n_0(x,y) \equiv n_0(x) \equiv n_0$ is the plasma density at the separatrix, and $\vec{V}$ is the perpendicular velocity due to the local $\vec{E} \times \vec{B}$ drift

$$\vec{V} = \frac{c}{B}\hat{e}_z \times \vec{\nabla}\phi \tag{3.4}$$

The continuity equation, for plasma density n, is

$$\left(\frac{\partial}{\partial t} + \vec{V} \cdot \vec{\nabla}\right)n = \frac{1}{e}\left(\hat{b} \cdot \vec{\nabla}\right)j_z \tag{3.5}$$

and the parallel component of the electron equation of motion (Ohm's law) leads to an equation for the vector potential, A_z,

$$\frac{\partial A_z}{\partial t} + c\left(\hat{b} \cdot \vec{\nabla}\right)\phi = \frac{cT_e}{en}\left(\hat{b} \cdot \vec{\nabla}\right)n \tag{3.6}$$

We consider the case of a strong toroidal magnetic field, $B_z \gg B_\perp$, and approximate the parallel gradients as $\hat{b} \cdot \vec{\nabla} \equiv \nabla_\parallel \approx \nabla_z$. This linearization of the parallel derivates means that we will not be able to capture the non-linear

interactions of Alfven waves, which are not of interest in the present study. We further make the assume that the parallel gradients have a length scale qR (and hence $k_{||} = (qR)^{-1}$), where q is the saffety-factor, so that the original 3-D system of equations is now reduced to 2-D. The reduced set of equations, derived from Eq.s 3.2–3.6 are

$$\frac{\partial}{\partial t}\left[n\left(\frac{\partial}{\partial t} + \vec{V}\cdot\vec{\nabla}\right)\nabla_\perp^2 \frac{e\phi}{T_e}\right] + \frac{\omega_{c_i}}{R}\frac{\partial}{\partial t}\left[\frac{\partial n}{\partial y}\right] = n_0\frac{V_A^2}{q^2 R^2}\nabla_\perp^2\left(\log n - \frac{e\phi}{T_e}\right) \quad (3.7)$$

$$\frac{\partial}{\partial t}\left[\left(\frac{\partial}{\partial t} + \vec{V}\cdot\vec{\nabla}\right)n\right] = \rho_s^2 n_0\frac{V_A^2}{q^2 R^2}\nabla_\perp^2\left(\log n - \frac{e\phi}{T_e}\right) \quad (3.8)$$

where $\omega_{c_i} = eB/Mc$ is the ion cyclotron frequency, and $V_A^2 = B^2/4\pi M n_0$ is the Alfven velocity.

3.1.1 Normalization scales

In order to perform computations of equations 3.7 and 3.8, we select normalization length and time scales such that all the physical process are of comparable time–scales. For normalization length, and time–scales of δ and τ respectively, this is equivalent to the constraint that all terms in equations 3.7 and 3.8 must be of comparable order of magnitude. Estimating the orders of the various terms in the two equations, we have

$$\underbrace{\frac{\partial}{\partial t}\left[n\frac{\partial}{\partial t}\nabla_\perp^2\frac{e\phi}{T_e}\right]}_{\frac{n}{\tau^2\delta^2}\frac{e\phi}{T_e}} + \underbrace{\frac{\partial}{\partial t}\left[n\vec{V}\cdot\vec{\nabla}\nabla_\perp^2\frac{e\phi}{T_e}\right]}_{\frac{cT_e}{eB}\frac{1}{\delta^2}\frac{n}{\tau\delta^2}\left(\frac{e\phi}{T_e}\right)^2} + \underbrace{\frac{\omega_{c_i}}{R}\frac{\partial}{\partial t}\left[\frac{\partial n}{\partial y}\right]}_{\frac{\omega_{c_i}}{R}\frac{n}{\tau\delta}} = \underbrace{n_0\frac{V_A^2}{q^2 R^2}\nabla_\perp^2\left(\log n - \frac{e\phi}{T_e}\right)}_{\frac{V_A^2}{q^2 R^2}\frac{n}{\delta^2}\frac{e\phi}{T_e}}$$

$$\underbrace{\frac{\partial}{\partial t}\left[\frac{\partial n}{\partial t}\right]}_{\frac{n}{\tau^2}} + \underbrace{\frac{\partial}{\partial t}\left[\vec{V}\cdot\vec{\nabla}n\right]}_{\frac{cT_e}{eB}\frac{1}{\delta^2}\frac{n}{\tau}\frac{e\phi}{T_e}} = \underbrace{\rho_s^2 n_0\frac{V_A^2}{q^2 R^2}\nabla_\perp^2\left(\log n - \frac{e\phi}{T_e}\right)}_{\rho_s^2\frac{V_A^2}{q^2 R^2}\frac{n}{\delta^2}\frac{e\phi}{T_e}}$$

Normalizing the electrostatic potential (ϕ) using the electron temperature (T_e), $\tilde{\phi} = e\phi/T_e$, and normalizing density using the separatrix density, n_0, we have

the constraints

$$\frac{1}{\tau^2\delta^2} \sim \frac{\rho_s c_s}{\tau\delta^4} \sim \frac{\omega_{c_i}}{R}\frac{1}{\tau\delta} \sim \frac{V_A^2}{q^2R^2}\frac{1}{\delta^2}$$

$$\frac{1}{\tau^2} \sim \frac{\rho_s c_s}{\tau\delta^2} \sim \frac{V_A^2}{q^2R^2}\frac{\rho_s^2}{\delta^2}$$

From the first set, we have,

$$\frac{1}{\tau^2\delta^2} \sim \underbrace{\underbrace{\frac{\rho_s c_s}{\tau\delta^4} \sim \frac{\omega_{c_i}}{R}\frac{1}{\tau\delta}}_{\delta^3 \sim \rho_s^2 R}}_{\tau \sim \frac{\delta^2}{\rho_s c_s}} \sim \frac{V_A^2}{q^2R^2}\frac{1}{\delta^2}$$

Thus, we arrive at the normalization length and time-scales of $\delta = \left(\rho_s^2 R\right)^{1/3}$ and $\tau = \omega_{c_i}^{-1}\left(R/\rho_s\right)^{2/3}$ respectively. Our normalized governing equations are

$$\frac{\partial}{\partial t}\left[n\left(\frac{\partial}{\partial t} + \vec{V}\cdot\vec{\nabla}\right)\nabla^2\phi\right] + \frac{\partial}{\partial t}\left[\frac{\partial n}{\partial y}\right] = n_0\Omega_A^2\nabla^2\left(\log n - \phi\right) \quad (3.9)$$

$$\frac{\partial}{\partial t}\left[\left(\frac{\partial}{\partial t} + \vec{V}\cdot\vec{\nabla}\right)n\right] = \left(\frac{\rho_s}{R}\right)^{2/3} n_0\Omega_A^2\nabla^2\left(\log n - \phi\right) \quad (3.10)$$

where we have omitted the $\tilde{()}$ signs as all variables are normalized. Here $\vec{V} = \hat{e}_z \times \nabla\phi$ is the normalized velocity, and $\Omega_A^2 = \left(\tau V_A/qR\right)^2$.

The aim of our normalization is to obtain a set of equation where interchange, drift and Alfven modes are of comparable time-scales. As we can notice in equations 3.9 and 3.10, the only free parameter in this system is the coefficient Ω_A^2 which depends on the tokamak operating parameters.

In table 3.1 we compute the value of Ω_A^2 for different tokamaks. We can see from the data that $\Omega_A^2 \sim 1$ for the existing tokamaks. We can see that all terms are of equal time–scales in the vorticity equations (Eq. 3.9). From the last row in table 3.1, we can see that the coefficient of the parallel term in the continuity equation(Eq. 3.10) is negligible. Hence, in the present work, we rewrite the continuity equation by neglecting the parallel contribution.

$$\frac{\partial}{\partial t}\left[\left(\frac{\partial}{\partial t} + \vec{V}\cdot\vec{\nabla}\right)n\right] = 0 \quad (3.11)$$

Table 3.1: Scales for different Tokamak parameters

	DIII-D	C-Mod	NSTX	ITER
R (cm)	175	70	85	620
q	3	3	3	3
n (cc^{-1})	$2 \cdot 10^{13}$	$7 \cdot 10^{13}$	$5 \cdot 10^{12}$	$1 \cdot 10^{14}$
c_s (cm/s)	$7 \cdot 10^6$	$6 \cdot 10^6$	$5 \cdot 10^6$	$1.2 \cdot 10^7$
ρ_s (cm)	$6.6 \cdot 10^{-2}$	$2.6 \cdot 10^{-2}$	$3.4 \cdot 10^{-1}$	$4.7 \cdot 10^{-2}$
δ(cm)	0.91	0.36	2.14	1.11
τ(s)	$1.8 \cdot 10^{-6}$	$8.4 \cdot 10^{-6}$	$2.7 \cdot 10^{-6}$	$2.2 \cdot 10^{-6}$
Ω_A^2	3.33	6.07	2.42	0.45
$\Omega_A^2 \left(\rho_s/R\right)^{(2/3)}$	$1.7 \cdot 10^{-2}$	$3.1 \cdot 10^{-2}$	$6.1 \cdot 10^{-2}$	$8.1 \cdot 10^{-4}$

3.1.2 Linear stability

We now consider the linear stabilty of our governing equations (Eq.s 3.9 & 3.11) for plasma whose equilibrium state is that of radially non–uniform density, $n(x,y) = n_0(x)$, and a uniform electrostatic potential, $\phi(x,y) = 0$. We assume that the perturbations ($\widetilde{n}(x,y)$ and $\widetilde{\phi}(x,y)$) can be described as a combination of travelling waves that can be described by their frequency (ω) and wave–number ($\vec{k}$), $\widetilde{(\ldots)} \sim exp\left(-i\omega t + i\vec{k} \cdot \vec{r}\right)$, and that the plasma gradient–scales are much larger than the perturbation length–scales.
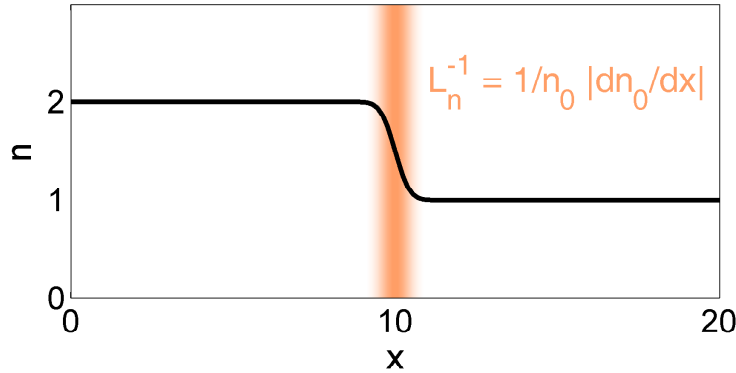
Figure 3.2: Schematic of the radial density profile

From the vorticity equation (Eq. 3.9) and continuity equaion (Eq. 3.11),

we obtain the following relations for the perturbed quantities

$$\omega^2 k^2 n_0 \widetilde{\phi} + \omega k_y \widetilde{n} = -n_0 \Omega_A^2 k^2 \left(\frac{\widetilde{n}}{n_0} - \widetilde{\phi} \right)$$

$$-\omega^2 \widetilde{n} - \omega k_y \frac{\mathrm{d}n_0}{\mathrm{d}x} \widetilde{\phi} = 0$$

leading to the dispersion relation,

$$\omega \left(\omega^2 + \frac{k_y^2}{k^2} L_n^{-1} - \Omega_A^2 \right) + \Omega_A^2 k_y L_n^{-1} = 0 \tag{3.12}$$

where $L_n^{-1} = n_0^{-1} \mathrm{d}n_0/\mathrm{d}x$ is the density gradient length–scale. In the above disper-
sion relation (Eq. 3.12), the second term $(k_y^2 L_n^{-1}/k^2)$ on the left hand side is the
interchange drive which has a destabilizing effect over the equilibrium profile that
corresponds to the outer side of the tokamak. The third term (Ω_A^2) corresponds
to the field–line stabilization which is of the form of Alfven waves. Electron drift–
waves are described by the third and fourth terms $(\Omega_A^2 L_n^{-1} k_y)$ in the dispersion
relation. From the second and third terms, we can see that the interchange drive
is stabilized by the field–line tension for

$$L_n^{-1} < \Omega_A^2 \tag{3.13}$$

In the present work, we consider plasma that is in a linearly stable equilib-
rium (Eq. 3.13). In the following sections we present the results of computational
investigation of the role of drift–wave turbulence, as described by equations 3.9
and 3.11, in the generation of blobs.

3.2 Numerical scheme

Our governing equations (3.9 and 3.11) are II–order in time. For conve-
nience in computations, we split each of the two governing equations into two
I–order equations (in time). For numerical stability during the computations, to
counter the dispersive truncation error in the numerical differencing scheme, we
add artificial diffusion terms $(D\nabla^2\dot{\Omega}, \nu\nabla^2\dot{n})$ to the time evolution equations that
require computation of gradients. Defining vorticity as $\Omega = \nabla^2\phi$, the rewritten

governing equations are

$$\frac{\partial \dot{\Omega}}{\partial t} = -\vec{V} \cdot \vec{\nabla}\dot{\Omega} - \dot{\vec{V}} \cdot \vec{\nabla}\Omega - \frac{\dot{n}}{n}\left(\dot{\Omega} + \vec{V} \cdot \vec{\nabla}\Omega\right) - \frac{1}{n}\frac{\partial \dot{n}}{\partial y}$$

$$+ \Omega_A^2 \nabla^2 \left(\frac{n}{n_{eq}} - \phi\right) + D\nabla^2 \dot{\Omega}$$

$$\frac{\partial \dot{n}}{\partial t} = -\vec{V} \cdot \vec{\nabla}\dot{n} - \dot{\vec{V}} \cdot \vec{\nabla}n + \nu\nabla^2 \dot{n}$$

$$\frac{\partial \Omega}{\partial t} = \dot{\Omega}$$

$$\frac{\partial n}{\partial t} = \dot{n} \tag{3.14}$$

where $\vec{V} = \hat{e}_z \times \vec{\nabla}\phi$ and $\dot{\vec{V}} = \hat{e}_z \times \vec{\nabla}\dot{\phi}$. To obtain ϕ, $\dot{\phi}$ from Ω, $\dot{\Omega}$ respectively, we need to solve the Poisson equations

$$\nabla^2 \phi = \Omega$$

$$\nabla^2 \dot{\phi} = \dot{\Omega} \tag{3.15}$$

The addition of artificial viscosity and diffusivity modify the linear dispersion relation of the governing equations. The dispersion relation of the equations 3.14 and 3.15 is

$$\omega\left(\omega^2 + \frac{k_y^2}{k^2}L_n^{-1} - \Omega_A^2 - k^4\nu D\right) + \Omega_A^2\left(k_y L_n^{-1} - ik^2\nu\right) = 0 \tag{3.16}$$

We can see from this dispersion relation that the artificial viscosity (ν) and diffusivity (D) have a stabilization effect in the competition between the interchange drive and field–line tension ($k^4\nu D$). Drift–waves are unstable in the present configuration, which is necessary for the growth of drift–wave turbulence.

Equations 3.14 are evolution equations in time. We use the numerical scheme described in section 3.2.2 to evolve these equations in time. We solve the equations 3.15 using a Poisson solver described in section 3.2.3.

3.2.1 Boundary Conditions

In order to solve the equations 3.14 and 3.15, we need information about the domain of interest, and the boundary conditions. The schematic of our computational domain with the boundary conditions is shown in Fig. 3.3. The Y–direction
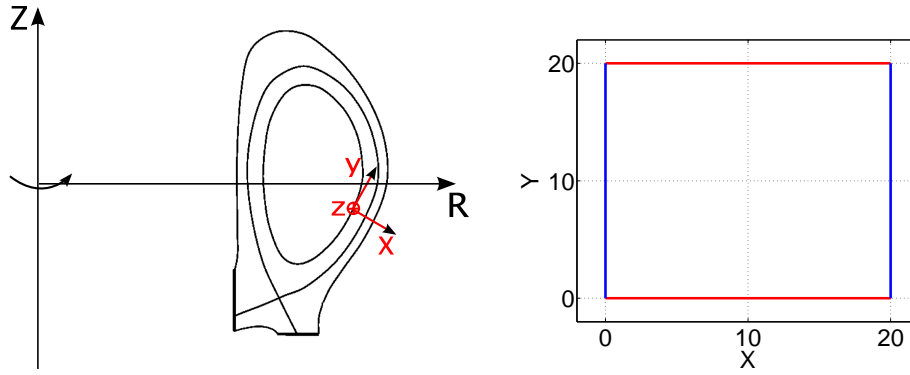
Figure 3.3: Boundary Conditions.

corresponds to the poloidal direction in a tokamak edge. Since the poloidal direction is a direction of periodicity, we treat the domain to be periodic in Y–direction. So all variables, and their first derivatives along Y are the same at the two Y– boundaries. For a variable denoted by f,

$$f|_{\text{upper bd.}} = f|_{\text{lower bd.}}$$
$$\left.\frac{\partial f}{\partial y}\right|_{\text{upper bd.}} = \left.\frac{\partial f}{\partial y}\right|_{\text{lower bd.}}$$

The X–direction corresponds to the radial direction in a tokamak edge. This is the direction of non–uniformity in the equilibrium plasma that forms the initial state for our computation. We apply a convective–boundary condition at the X– boundaries.

$$\left.\frac{\partial f}{\partial x}\right|_{\text{left bd.}} = 0$$
$$\left.\frac{\partial f}{\partial x}\right|_{\text{right bd.}} = 0$$

Since diffusive flux is proportional to the gradient, the physical significance of our boundary condition is that fluxes at the boundary are convective.

3.2.2 Advancing in time: RKW3 scheme

In our computations, we use the Runge Kutta-Wray (RKW3) method ([39]) for the time evolution of equations 3.14. The standard Runge Kutta methods

require temporary variables for intermediate stages in the time–evolution at each time–step. The RKW3 method is an elegant III–order method of the Runge Kutta family of methods that has low memory storage requirements, and hence is computationally efficient. In this method, we march the equation

$$\frac{\mathrm{d}y}{\mathrm{d}t} = f(y, t)$$

from the nth to $(n+1)^{th}$ time–step (of magnitude h) as

$$
\begin{aligned}
k_1 &= f(y_n, t_n) \\
k_2 &= f(y_n + \beta_1 h k_1, t_n + \alpha_1 h) \\
k_3 &= f(y_n + \beta_2 h k_1 + \beta_3 h k_2, t_n + \alpha_2 h) \\
y_{n+1} &= y_n + \gamma_1 h k_1 + \gamma_2 h k_2 + \gamma_3 h k_3
\end{aligned}
\tag{3.17}
$$

where the coefficients are

$$
\begin{aligned}
\beta_1 &= 8/15, \quad \beta_2 = 1/4, \quad \beta_3 = 5/12, \\
\alpha_1 &= 8/15, \quad \alpha_2 = 2/3, \\
\gamma_1 &= 1/4, \quad\quad \gamma_2 = 0, \quad\quad \gamma_3 = 3/4
\end{aligned}
$$

We can see, from Eq. 3.17 that there are three temporary variables per time–step. The advantage with RKW3 method is that, in practice the time–stepping will require only one temporary variable per equation, thereby reducing the memory requirement for the time–stepping by a third. In practice the time–stepping(Eq. 3.17) is re-written in a low memory–storage form having a temporary variable k,

$$
\begin{aligned}
k &= f(y, t_n) \\
y &= y + \beta_1 h k \\
k &= y + \zeta_2 h k \\
y &= f(y, t_n + \alpha_1 h) \\
k &= k + \beta_3 h y \\
y &= k + \zeta_3 h y \\
k &= f(k, t_n + \alpha_2 h) \\
y &= y + \gamma_3 h k
\end{aligned}
\tag{3.18}
$$

where $\zeta_2 = -17/60$ and $\zeta_3 = -5/12$. Clearly, the above numerical scheme has only one temporary variable, k, unlike the original form (Eq. 3.17) which has three temporary variables, k_1, k_2 and k_3. For a computational domain with 128×128 grid points, this reduction of storage requirement by a factor of 3 reduces the computation cost significantly.

3.2.3 Poisson equation

Our time–evolution equations are for vorticity ($\Omega = \nabla^2 \phi$) and density (n). However, to obtain the velocity of plasma ($\vec{V} = \hat{e}_z \times \vec{\nabla} \phi$), we need to obtain the electrostatic potential (ϕ) from the voriticty (Ω). This involves the solution of the Poisson equations (Eq. 3.15) which are of the form

$$\nabla^2 u = v \tag{3.19}$$

Since our domain is periodic along the Y–direction, $u(x, y)$ and $v(x, y)$ can be treated as periodic over the domain along Y

$$u = \sum_{m=0}^{N_y/2-1} \hat{u}_m(x) e^{im2\pi y/L_y}$$

$$v = \sum_{m=0}^{N_y/2-1} \hat{v}_m(x) e^{im2\pi y/L_y}$$

where $\hat{u}_m$ and $\hat{v}_m$ are complex quantities (with both real and imaginary components), which can be obtained by taking the Fourier transforms of u and v. Our Poisson equation (Eq. 3.19) is now of the form

$$\sum_{m=0}^{N_y/2-1} \frac{\partial^2 \hat{u}_m(x)}{\partial x^2} e^{im2\pi y/L_y} - \sum_{m=0}^{N_y/2-1} \frac{m^2 \pi^2}{L_y^2} \hat{u}_m(x) e^{im2\pi y/L_y} = \sum_{m=0}^{N_y/2-1} \hat{v}_m(x) e^{im2\pi y/L_y}$$

which is a set of N_y decoupled 1–D equations in x

$$\frac{\partial^2 \hat{u}_m(x)}{\partial x^2} - \frac{m^2 \pi^2}{L_y^2} \hat{u}_m(x) = \hat{v}_m(x) \tag{3.20}$$

for $m = 0$ to $N_y/2 - 1$.

Equations 3.20 are II–order equations in 1–dimension, and their numerical solution is straight–forward. Taking the inverse Fourier transform of the $\hat{u}_m$'s obtained by solving Eq. 3.20 gives us the solution for the Poisson equation 3.19.

3.3 Initial condition

We consider an equilibrium plasma that is uniform in the poloidal direction and is non–uniform radially, $n(x, y) = n_0(x)$. This density profile, shown in Fig. 3.4, is characterized by its peak radial gradient: $L_n^{-1} = 1/n_0 \mathrm{d}n_0/\mathrm{d}x$. We choose

(a) 2-D plot of density

(b) Poloidally averaged density
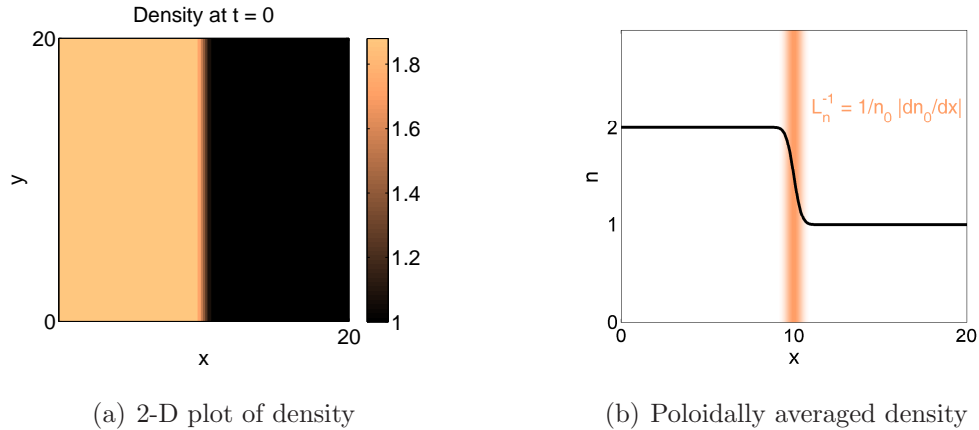
Figure 3.4: Illustration of the initial condition.

our initial condition such that the interchange drive is stabilized by the field–line tension, following the linear dispersion relation (Eq. 3.12),

$$\omega \left(\omega^2 + \frac{k_y^2}{k^2} L_n^{-1} - \Omega_A^2 \right) + \Omega_A^2 k_y L_n^{-1} = 0$$

We see from the above dispersion relation that both field–line stabilization and drift–wave terms are dependent on Ω_A^2, which is the only parameter in our governing equations that is determined by details of the existing magnetic confinement devices. Based on the comparison done in table 3.1, we see that $0.3 < \Omega_A^2 < 10$. In the following section, we present the results of computations performed for different values of Ω_A^2 that fall in this range.

Our goal is to verify whether the non–linear interaction of drift–waves in such a configuration leads to the generation of blobs. We perform this by seeding a density perturbation that sets-off drift–waves in the plasma that is initially quiescent. We ensure that the density perturbation is sufficiently large for the ensuing drift–waves to be of non–negligible magnitude at the beginning of the simulation. The perturbation is of the form of a Guassian that is localized in both x and y

directions. We evolve the perturbed plasma long enough for the interaction of drift–waves to be nonlinear inorder to verify whether the nonlinear interactions lead to a spilling–off of blobs.

3.4   Results & Discussion
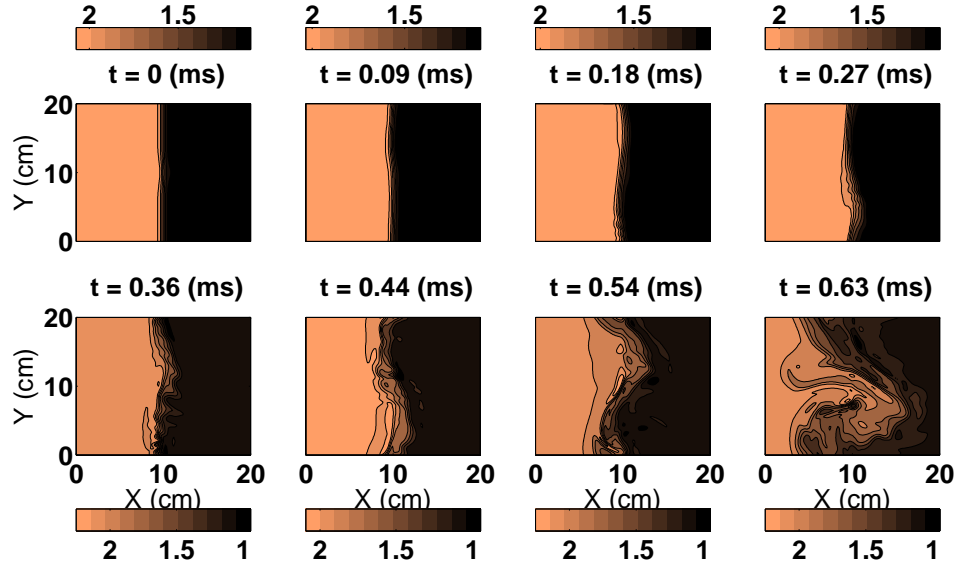
Figure 3.5: Simulation results for $\Omega_A^2 = 1.0$, $L_n^{-1} = 0.7$

We first consider a configuration represented by the parameter $\Omega_A^2 = 1.0$. In Fig. 3.5, we show the evolution of a perturbed plasma whose density variation scale is $L_n^{-1} = 0.7$. This initial condition is linearly stable according to Eq. 3.12. In Fig. 3.5 we show contour plots of density at different stages of time evolutions. We can see that the perturbation sets–off drift–waves that propagate poloidally. Drift–waves are unstable in the configuration, and hence they grow by deriving energy from the plasma density gradient. We observe that the small–wavenumber motions gain energy over time resulting in the formation of a meso–scale structure.

We also consider a configuration represented by $\Omega_A^2 = 3.0$, corresponding to a DIII-D plasma. We begin with a radial density profile whose density variation scale is given by $L_n^{-1} = 1.2$, which is linearly stable due to the effect of the field–line
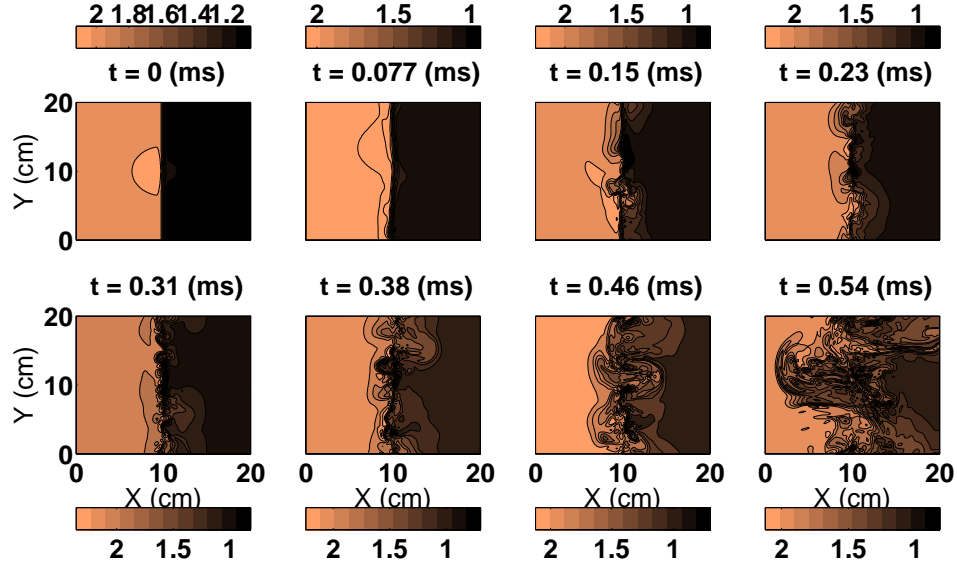
Figure 3.6: Simulation results for $\Omega_A^2 = 3.0$, $L_n^{-1} = 1.2$

tension according to Eq. 3.12. As seen in Fig. 3.6, the qualitative evolution in this case is similar to that observed in Fig. 3.5.

In the previous two cases, we observe that energy is gained the most by the lowest wave–number motions in the turbulent fluctuations. It should be noted that our assumptions regarding the variation of magnetic field imposes an upper limit on the poloidal extent of our domain, and hence the size of the meso–scale structure. Since we are simulating turbulent fluctuations, in order to verify the adequate resolution of the small scale motions, we performed additional computations using a refined mesh (256×256) over a smaller domain (10×10). The results, as shown in Fig. 3.7, confirm that the simulations shown in figures 3.5 and 3.6 adequately resolve the drift–wave turbulence of interest.

3.5   Conclusions

In this chapter we have demonstrated, using numerical simulations, that even in a configuration where the interchange drive in the bad curvature region is stabilized by the field–line tension due to the connection with the region of
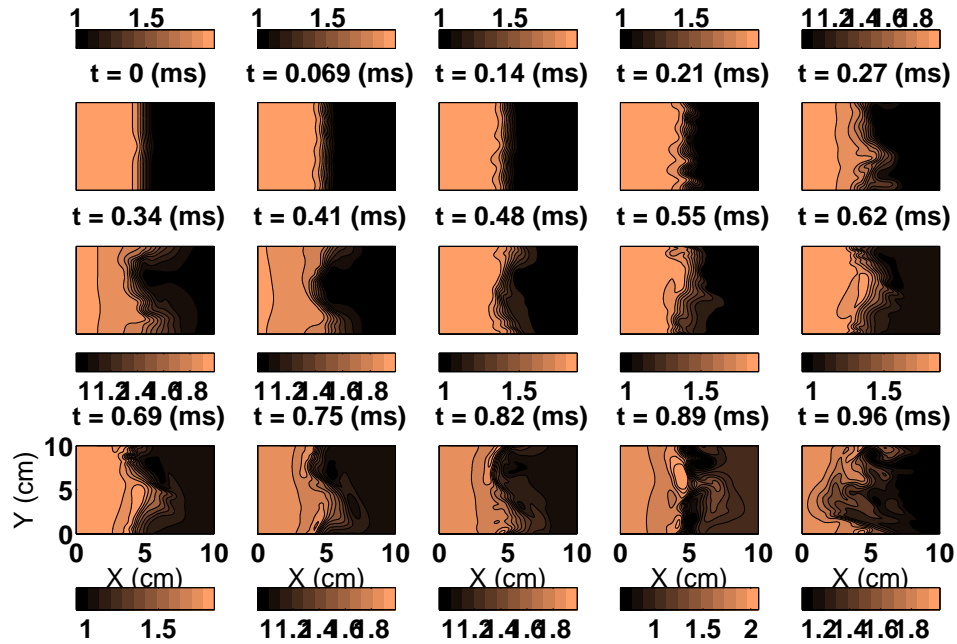
Figure 3.7: Simulation results for $\Omega_A^2 = 1.0$, $L_n^{-1} = 0.65$

good–curvature, the Reynolds stresses due to drift–wave turbulence lead to the generation of blobs. Fig. 3.8 illustrates the mechanism of generation of blobs. The green curve represents the equilibrium plasma whose gradients are not steep enough to overcome the stabilization due to connection with the region of good curvature. The red curve represents the large–scale structures, arising out of the drift–wave turbulence due to the inverse cascade, that are unstable under the interchange drive.

The results presented in chapter 3 have been published in "On the mechanisms of generation of meso-scale convective structures in tokamak edge plasma", K. Bodi, S. I. Krasheninnikov, and A. I. Smolyakov, Contributions to Plasma Physics, 48(1-3):6367 (2008) and "On blob generation mechanisms in tokamak edge plasma", K. Bodi, A.I. Smolyakov, and S.I. Krasheninnikov, Journal of Nuclear Materials, 390-391:359 (2009). The dissertation author was the primary author of these publications.
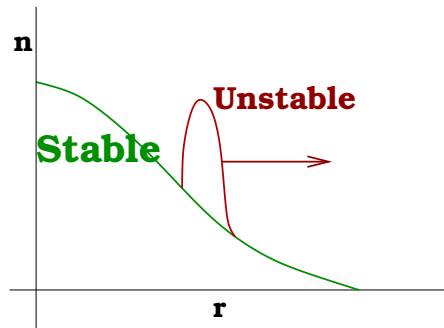
Figure 3.8: Cartoon illustration of the mechanism of blob generation

Chapter 4

Blob dynamics in inhomgeneous plasma

4.1   Introduction

Cross-field transport of magnetically confined plasmas in so-called Scrape off Layer (SOL) (e.g. in tokamaks and helical devices) and "shadow"(e.g. in linear devices) regions is characterized by intermittent radial convection of filamentary meso-scale plasma structures elongated along the magnetic field lines and often called "blobs" (e.g., see [11–17, 40–44]).

It is widely accepted that in tokamaks and helical devices an effective gravity, caused by inhomogeneous magnetic field, is the reason for the convective motion of such meso-scale structures ([6, 8]). In linear devices, an effective gravity can be associated with so-called "neutral wind" effects [45].

However, in [46] it was shown that nonlinear cross-field advection of plasma structures can be associated with the effects related to instabilities driven by ∇T_e and parallel shear of $\vec{E} \times \vec{B}$ drift velocity. Although such structures exhibit wedge-like cross-field shape it is conceivable that isolated blobs can detach from the tip of the wedge due to some other effects (e.g. sheared plasma flow) and after that propagate further just by inertia. Other driving forces can, probably, also result in some nonlinear effects, which finally cause "spilling" of blobs into SOL/"shadow"

region where they can propagate further by inertia even in the absence of effective gravity. Such physical picture would explain, for example, the observation of blob motion in linear devices without involving the "neutral wind" effects.

Such inertial motion of a blob in homogenous magnetic field, $\vec{B} = \hat{e}_z B$ ($B = $ const. and $\hat{e}_z$ is the unit vector), can be described by the following two dimensional $(2-D)$ vorticity equation of incompressible cross-field plasma flow (e.g. see Ref. 14 and the references therein)

$$\vec{\nabla} \times \left(\rho \frac{\mathrm{d}\vec{V}}{\mathrm{d}t} \right) = \mu \nabla^2 \left(\vec{\nabla} \times \vec{V} \right) + \frac{1}{cL_b} \int \left(\vec{B} \cdot \vec{\nabla} \right) \vec{j} \mathrm{d}z \qquad (4.1)$$

where: $(\mathrm{d}/\mathrm{d}t)(\dots) = \left(\partial/\partial t + \vec{V} \cdot \vec{\nabla} \right)(\dots)$, $\vec{V} = (c/B)\,\hat{e}_z \times \vec{\nabla}\phi$, ρ , and μ are the plasma cross-field velocity, mass density and viscosity respectively (we assume here that); ϕ is the electrostatic potential; $\vec{j}$ is the vector of electric current, L_b is the blob length along the magnetic field, and c is the speed of light.

The terms on the right side of Eq. 4.1 cause the dissipation of plasma vorticity and slow down the blob motion. As a result, blob can penetrate into SOL/"shadow" region only on some distance L_{pen}, which is determined by the initial blob speed and viscosity dissipation rate. For example, for the case where dissipation is caused by parallel current flowing through the sheath, the distance L_{pen} can be estimated as follows [8]:

$$L_{pen} \sim L_b \frac{e\phi_0}{T} \frac{n_b}{n_{sh}} \left(\frac{\rho_s}{a_b} \right)^3 \qquad (4.2)$$

where ϕ_0 is the initial magnitude of electrostatic potential variation in the blob, T is the plasma temperature, n_b and n_{sh} are the plasma density in the blob and in the sheath, ρ_s is the effective ion Larmor radius, and a_b is the cross-field size of the blob. For typical conditions of [44] $L_b \sim 500$cm, $\rho_s/a_b \sim 0.2$, assuming that $e\phi_0/T \sim 1$ and $n_b/n_{sh} \sim 3$, from Eq. 4.2 we find $L_{pen} \sim 10$cm.

As we see, just by inertia blob can penetrate into SOL/"shadow" region on a distance, which can significantly exceed the characteristic scale length of background plasma mass density decay $L_\rho = |\nabla \log (\rho_{bg})|^{-1}$. However, motion of the blob involves the motion of surrounding plasma as well. If we ignore dissipative effects, total energy of plasma flow including inside and outside blob should be

conserved. Then, the variation of the background plasma density in the vicinity of the blob will alter the energy of the outside flow and, therefore, should affect blob dynamics. Such effect was largely ignored in previous studies of blob physics, in particular, for the reason of the usage of the Boussinesq approximation in vorticity equation Eq. 4.1, where derivative of mass plasma density in the left hand side of Eq. 4.1 was often omitted, but which breaks the conservation of energy. We notice that the Boussinesq approximation is often used in numerical modeling of edge plasma turbulence. In what follows we will consider the effects of the variation of background plasma density on blob dynamics using exact vorticity equation.

4.2 Effect of background density on blob propagation

In the simplest case, where the main vorticity dissipation is due to viscous effects, Eq. 4.1 combined with the continuity equation

$$\frac{\mathrm{d}\rho}{\mathrm{d}t} = D\nabla^2 \rho \tag{4.3}$$

where D is the diffusion coefficient, describes 2D motion of an incompressible fluid. If both D and μ are rather small, we can neglect dissipation effects. As a result the problem of blob motion in inhomogeneous magnetized plasma becomes identical to the inviscid motion of fluid dipolar vortex structure through a background fluid with varying mass density. The stream function of such fluid flow is shown schematically in Fig. 4.1 in a moving frame. For simplicity we assume here that the dipolar vortex has cylindrical shape and the separatrix of radius separates internal and external flows.

The problem of inviscid flow of fluid with a weak mass density gradient (which in our case it corresponds to the inequality $\varepsilon \equiv a_b \left|\nabla \log\left(\rho_{bg}\right)\right|^{-1} \equiv a_b/L_\rho \ll 1$) around bodies was considered recently in [47]. Analyzing both continuity and momentum balance equations for $\varepsilon \ll 1$ it was shown, in particular, that for the case where body moves in parallel direction to the gradient of background density,
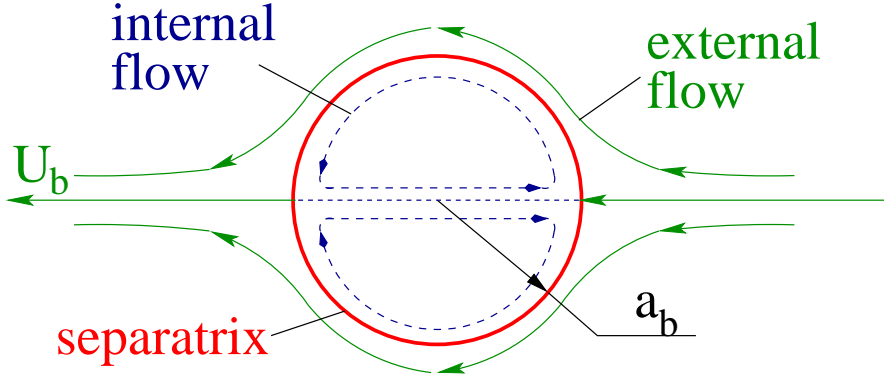
Figure 4.1: Schematic view of plasma flow stream function in a blob (moving frame)

there is a force, $\vec{F}$, acting on the body:

$$\vec{F} = -CW\left(\vec{U} \cdot \vec{\nabla}\rho_{bg}\right)\vec{U} \tag{4.4}$$

where W and $\vec{U}$ are the volume and the velocity of the body, and C is the coefficient which depends on the shape and the orientation of the body. For example, for the cylinder moving perpendicular to its axis $C = 0.5$. For the cylinder moving with the constant speed U_c the expression (4.4) can be easily recovered just from the energy balance equation. Indeed, to describe fluid flow around the cylinder with radius a_c moving perpendicular to its axis in zero order approximation over parameter $\varepsilon \ll 1$, we can use the flux function, $\Psi(x, y)$, corresponding to homogeneous fluid, which in the moving frame is (e.g. see [48])

$$\Psi = -U\left(r - \frac{a_c^2}{r}\right)\sin\theta \tag{4.5}$$

where we use polar coordinates assuming that the cylinder moves along x-coordinate. We notice that this flow corresponds to the external flow of blob (see Fig. 4.1). Then we find that in the laboratory frame the kinetic energy of the fluid flow around the cylinder per unit length, E_{ext}, is

$$E_{ext}(x_c) = \frac{\pi}{2}\rho_{bg}(x_c)U_c^2 a_c^2 \tag{4.6}$$

where $x_c(t)$ is the x-coordinate of the center of the cylinder. Because total energy of the cylinder and surrounding fluid should be conserved, we come the following

energy balance equation:

$$\int_{x_c(t_0)}^{x_c(t)} F \mathrm{d}x = E_{ext}(x_c(t_0)) - E_{ext}(x_c(t)) \tag{4.7}$$

where t_0 is just some reference time. Taking into account 4.6, and differentiating 4.7 over time, while assuming $U = \text{const.}$, we come to the expression

$$F(x) = -\frac{\pi}{2}\frac{\mathrm{d}\rho_{bg}}{\mathrm{d}x}U_c^2 a_c^2 \tag{4.8}$$

which is identical to Eq. 4.4 for the cylinder.

In order to get an insight on the impact of the variation of background plasma density on blob dynamics we will follow [47] and assume that the ratio a_b/L_ρ is small, even though in practice it may not be applicable.

We assume that the dipolar structure of the blob has cylindrical form of radius a_b. In contrast to the motion of solid cylinder, blob's plasma has both external and internal flows, which can be charaterized by the energies E_{ext} and E_{int} (in moving frame) respectively. In addition ot that we should account for the energy associated with ballistic motion of internal region of the blob with speed U_b: $E_U = \frac{\pi}{2}\rho_b U_b^2(x)a_b^2$ (ρ_b is the plasma mass density inside the separatrix). Then, neglecting dissipative effects we arrive to the following expression for the balance of energy per parallel length of the blob

$$E_{ext} + E_{int} + E_U = \text{const.} \tag{4.9}$$

where E_{ext} and E_{int} are the energy of external and internal blob plasma flows (see Fig. 4.1) and E_U is the energy associated with ballistic motion of the blob (ρ_b is the plasma mass density inside the separatrix). From Eq. 4.6 we find $E_{ext} = \frac{\pi}{2}\rho_{bg}(x)U_b^2(x)a_b^2$. In the absence of dissipation both ρ_b and E_{int} remain to be constant $\rho_b = \rho_b(x_0)$ and $E_{int} = C_0\rho_b(x_0)U_b^2(x_0)a_b^2$, where x_0 is the coordinate where blob was generated and C_0 is the coefficient taking into account the details of internal plasma flow.

Then, from Eq. 4.9 we find

$$U_b(x) = U_b(x_0)\left(\frac{\rho_{bg}(x_0) + \rho_b}{\rho_{bg}(x) + \rho_b}\right)^{1/2} \tag{4.10}$$

As we see from Eq. 4.10, a blob propagating into SOL/"shadow" region with low plasma density accelerates, while blob moving in opposite direction slows down. To estimate maximum gain of blob speed we assume in Eq. 4.10 that $\rho_b(x_0) \approx \rho_{bg}(x_0) \gg \rho_{bg}(x)$, which gives $\max\left(U_b(x)/U_b(x)\right) = \sqrt{2}$.

So far we neglect dissipative processes. However, both blob motion in inhomogeneous background plasma and the variation of blob speed, will cause strong gradients at the interface between inner dipolar structure and outside flow, which can enhance dissipation and make our estimations of blob dynamics inapplicable.

In order to estimate the effects of dissipation, let us assume that the dissipation is due to viscosity and diffusion and $D \widetilde{<} \nu \equiv \mu/\rho$. First we notice that blob remains coherent structure and is not dissipated while moving over distance of interest, $L_\rho \sim |\nabla \log \rho_{bg}|^{-1}$, if

$$\mathrm{Re}' = \frac{a_b}{L_\rho}\mathrm{Re} \equiv \frac{a_b}{L_\rho}\frac{U_b a_b}{\nu} \gg 1 \tag{4.11}$$

Next, the characteristic width of a strong velocity gradient, δ, can be estimated as follows $\delta \sim \sqrt{\nu L_\rho/U_b}$. As a result, we find the energy per parallel length dissipated while blob moved at the distance $\sim L_\rho$:

$$E_{visc} \sim \nu \rho_b \left(\frac{U_b}{\delta}\right)^2 \delta a_b \frac{L_b}{U_b} \tag{4.12}$$

Comparing this energy loss with total energy of the blob $E_b \sim \rho_b U_b^2 a_b^2$ we find

$$\frac{E_{visc}}{E_b} \sim \frac{1}{\sqrt{\mathrm{Re}'}} \tag{4.13}$$

Thus we conclude that for large values of Re' we can ignore dissipation and use the kinetic energy conservation. However, we should notice that at very large Reynolds numbers (Re larger than few thousand) the Kelvin-Helmholtz instability should be taken into account, which will significantly alter the dynamics of blobs.

4.3   Numerical Simulations

Computations were carried out to demonstrate the above conclusions. We solve 2D vorticity and continuity equations of incompressible plasma flow in (x, y)
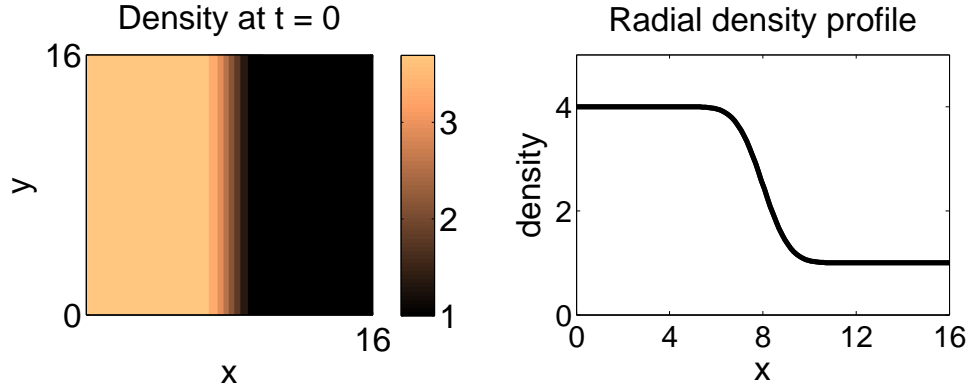
Figure 4.2: Initial plasma density profile.

plane, which in dimensionless units have the form

$$\frac{\partial \Omega}{\partial t} + \vec{V} \cdot \vec{\nabla}\Omega + \hat{e}_z \cdot \left(\vec{\nabla}\tilde{E} \times \vec{\nabla}n \right) = \tilde{\nu}\nabla^2\Omega \tag{4.14}$$

$$\frac{\partial n}{\partial t} + \vec{V} \cdot \vec{\nabla}n = \tilde{D}\nabla^2 n \tag{4.15}$$

where n and $\vec{V} = \hat{e}_z \times \vec{\nabla}\phi$ are the dimensionless plasma density and velocity, ϕ is the electrostatic potential,

$$\Omega = \vec{\nabla} \cdot \left(n\vec{\nabla}\phi \right) \tag{4.16}$$

is the generalized vorticity, and $\tilde{E} = |\nabla\phi|^2/2$; $\tilde{\nu}$ and $\tilde{D}$ are the dimensionless kinematic viscosity and diffusion coefficients.

We solve Eq. 4.15 by using third order Runge-Kutta scheme (RKW3 Scheme is described in section 3.2.2). We obtain the electrostatic potential ϕ by iteratively solving the nonlinear Poisson equation (Eq. 4.16) using a Successive-OverRelaxation (SOR) method,

$$\phi^{(n+1)} = (1 - \omega)\phi^{(n)} + \omega\Delta^{-1}\left(\frac{\Omega}{n} - \frac{1}{n}\vec{\nabla}n \cdot \vec{\nabla}\phi^{(n)} \right) \tag{4.17}$$

with $\omega = 1.2$, and inversion of the Laplacian, Δ^{-1}, was done using a Fourier method (Poisson Solution is described in section 3.2.3).

We seed blobs as the perturbations of ϕ ($\max(|\phi|) = 1.0$) by specifying a vorticity dipole with dimensionless radius 0.5 and use non-uniform background density (see Fig. 4.3, top) with characteristic dimensionless $L_\rho \sim 3$. A schematic

of the initial density profile is shown in Fig. 4.2. We take $\tilde{\nu} = \tilde{D} = 10^{-3}$, so that $\mathrm{Re}' \sim 10^2 \gg 1$. Such a vortex dipole moves along the x-coordinate.

In Fig. 4.3 (bottom) we show the coordinates of "center of mass" of the blobs as a function of time for a blob initially moving towards increasing density (curve 1), a blob moving towards decreasing density (curve 2), and the dotted lines correspond to inward and outward moving blobs in unifrom density plasma. The
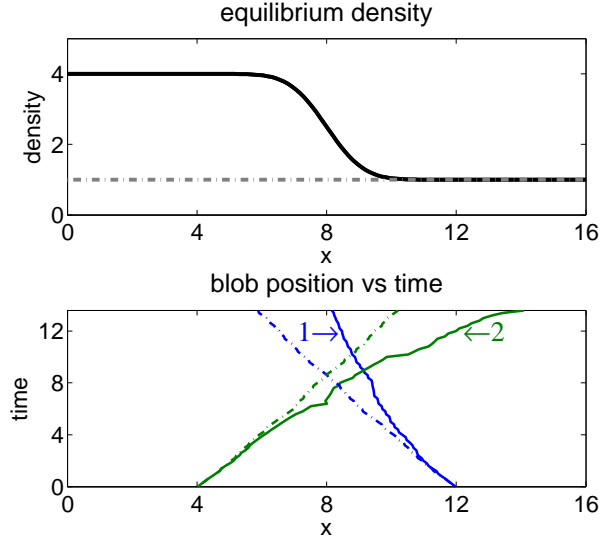
Figure 4.3: Effect of density gradient on blob propagation. Top: Equilibrium density profile. Bottom: Coordinates of "center of mass" of the blobs as a funciton of time.

contour plots of the magnitude of the potential ϕ are shown in Fig. 4.4 for: a blob moving along increasing density (a), a blob moving through uniform density (b), and a blob moving along decreasing density (c).

The density evolution is shown in Fig. 4.5 for: a blob moving along increasing density (top) and a blob moving along decreasing density (bottom).

4.4 Conclusions and discussions

We have shown that the impact of equilibrium plasma density variation on the propagation of seeded blobs (no interchange drive) is in the form of a clear
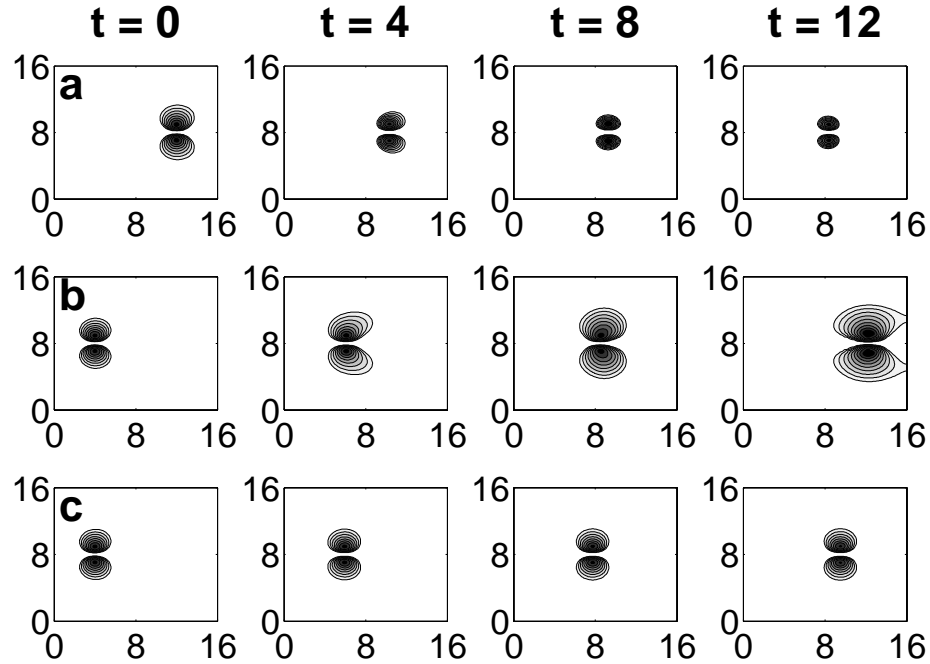
Figure 4.4: Contours of electrostatic potential ϕ for blobs moving along x-direction: a) a blob moving through uniform density, b) a blob moving through decreasing density, and c) a blob moving through increasing density.

preference for blobs propagating into low plasma density, suggesting the convective nature of non-uniform plasma transport. This is the result of the equilibrium plasma density gradient affecting the vorticity balance. A sink/source term due to the equilibrium plasma density gradient in the vorticity balance equation affects the energy balance via the redistribution of the energy between the inner and our part of the blob. Note that the total energy conservation includes the energy of the plasma motion outside the blob. This "wake" region ([47]) (the size of this region is of the order of the blob radius) is crucial for the mechanism of the blob acceleration/de-acceleration in inhomogenous plasma ([47]).

It is interesting to note that effects of the equilibrium plasma gradient beyond Boussinesque approximation are naturally responsible for the asymmetry of the propagation of drift waves with respect to the density gradient direction. One can expect that such effects will lead to the asymmetry of the drift-wave spectra in fully developed turbulent state in a tokamak and, correspondingly, to the net
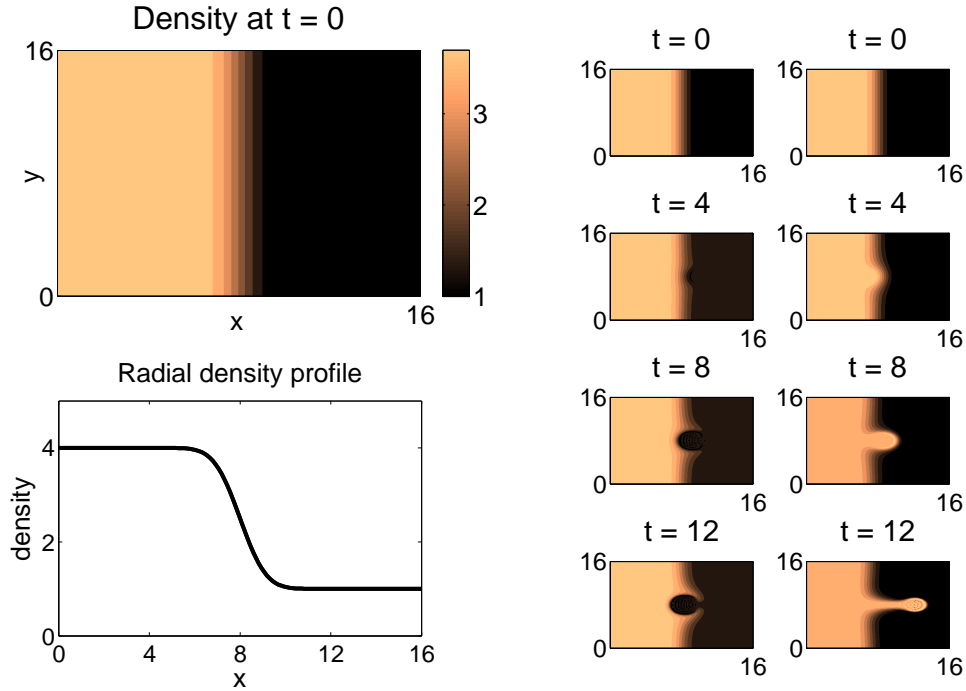
Figure 4.5: Density evolution for a blob moving along x-direction: along increasing density (top), and for a blob moving along decreasing density (bottom).

radial propagation of fluctuations ([49, 50]). Radial drift wave propagation toward the plasma edge was earlier proposed as a source of plasma edge turbulence in [51] where the effects of decreasing plasma density toward the edge were responsible for the enhance turbulence level at the edge. In general blobs have to considered as a nonlinear self-consistent state including both plasma and wave motion, or in other words, blobs correspond to the strongly nonlinear state of drift wave turbulence with substantial amount of plasma trapped inside the vorticies. Therefore, the blob acceleration studied in the paper is an effect complementary to that considered in [51].

Chapter 4, in full, is a reprint of the material as it appears in "Blob dynamics in an inhomogeneous plasma", K. Bodi, S. I. Krasheninnikov, and A. I. Smolyakov, published in Physics of Plasmas, 15(10):102304 (2008). The dissertation author was the primary author of this publication.

Chapter 5

Kinetic code for edge plasma transport simulation

The edge region of tokamak plasma is the region of transition between the hot core and the external vacuum, and hence it is the region of gradients of plasma properties (density, temperature etc). As the collision mean free path depends quadratically on the local temperature, we expect the plasma to be increasingly collisional from core radially outward across the edge. For plasma configurations with sharp gradients at the edge (like in H–mode) there is no significant scale–separation between the particle drift orbits and gradient lengthscales. Though the gradients are less steep in the L–mode plasmas, the edge region in such configurations consists of large magnitude turbulent fluctuations($e\langle\phi\rangle_{rms}/T \sim 1$, see [52]). An additional feature of edge plasma, in contrast to the core, is the presence of intermittent structures like blobs (observed in L–mode) and ELMS (H–mode) whose magnitude is comparable to (or larger than) that of the edge plasma [8]. The edge region, therefore, consists of large variations leading to local distribution functions that may deviate significantly from a Maxwellian state.

In a tokamak plasma, the particle time–scales range from that of the particle cyclotron rotation time–scales (shortest) to that of the plasma confinement time–scales (longest). Most often, we are interested in the transport processes that determine the plasma profiles and confinement durations. To numerically simulate a process, the magnitude of time–step in the numerical evolution must be smaller

than the time–scale of the process. Hence, if we aim to resolve all the processes involved, computing time evolution using the kinetic equation is not practicable even with most powerful supercomputers. For computational convenience, we average out the fastest processes (particle cyclotron motions), and thereby reduce the range of time–scales that need to be resolved by our computations. The resulting governing equations are called the *gyrokinetic* equations [53].

5.1 TEMPEST

The kinetic simulations reported in the present chapter, and chapter 6, were performed using the gyrokinetic code TEMPEST. TEMPEST is a gyrokinetic code for edge plasma simulations. It is a five dimensional (ψ, θ, ζ, $\mathcal{E}_0$, μ) continuum code that represents the velocity space as a grid in equilibrium energy ($\mathcal{E}_0$) and magentic moment (μ) variables, and the configuration space as a grid in magnetic flux–surface (ψ), poloidal angle (θ), and toroidal angle (ζ). In addition to being able to perform computations on annulus-like edge geometries (closed fieldlines), TEMPEST is capable of handling the geometry of a diverted tokamak (closed and open fieldlines). A description of the governing equations and numerical schemes in TEMPEST can be found in [9]. In its full 5–D form, TEMPEST can perform turbulence calculations for edge plasma. Alternately TEMPEST can be run as a 4–D (ψ, θ, $\mathcal{E}_0$, μ) transport code that can simulate neoclassical transport due to particle drifts in edge plasma.

The magnetic field configuration in a tokamak is aimed at nullifying transport across flux–surfaces. While radial flux due to particle drifts normal to the flux–surfaces is finite locally, the net flux normal to given flux–surface (obtained as an average of the flux at all poloidal locations over the flux–surface) vanishes due to the magnetic geometry. Satisfying this constraint is necessary for magnetic confinement of plasma. While this constraint is satisfied exactly in the idealization of a collisionless plasma, there exists a finite flux normal to the flux–surfaces in the presence of collisions. In contrast to the classical transport, arising out of the collisions between the random (Brownian) motion of particles in plasma, transport

arising out of collisions between particles undergoing charged-particle drifts (due to the tokamak electric- & magnetic–fields) is known as *neo–classical* transport [3]. Thus, to compute transport due to particle drifts, an effective collision model is needed along with particle drift computations in the kinetic code. As a first step in this direction, we have implemented a Krook collision model.

5.2   Krook collision model for TEMPEST

Krook collision model [54] is of the form

$$\left. \frac{\partial f}{\partial t} \right|_c = -\nu_k \left(f - f_M \right) \tag{5.1}$$

where f_M is a Maxwellian distribution with the same values of density (n) and temperature (T) as that of the distribution function, f. Thus, for a particle density conserving Krook collision model, the zeroeth moment of f_M should match that of f. For a particle and energy conserving model, the zeroeth and second moments of f_M must match that of f. The coefficient ν_k contains the collisional time–scale at which the distribution function relaxes to a Maxwellian state.

5.3   Implementation

To compute the Krook collision term that satisfies particle density and energy conservation, we need to define a Maxwellian distribution function corresponding to the density and energy of the species as computed from the species distribution function. In practice, since the moments are computed using numerical integration of the particle distribution functions, care should be taken to avoid loss of conservation properties due to the errors in the numerical quadrature. The nature of this error can be illustrated by considering the case of a species of particle and energy densities of n_0 and $n_0 T_0$ respectively. We define the species distribution function (f_0) as a Maxwellian distribution of these particle and energy densities. To compute the collision term in the kinetic equation, which should vanish for a Maxwellian, we first compute the particle and energy densities of the

distribution function. Due to the errors in the quadrature scheme, the computed particle and energy densities are n_1 and $n_1 T_1$. Denoting the reference Maxwellian for the collision term with f_{M_0}, we have,

$$\left.\frac{\partial f_0}{\partial t}\right|_c = -\nu_k \left(f_0 - f_{M_0}\right) \tag{5.2}$$

Taking moments of the above equation, we obtain the following equations for particle and energy desnsity conservation,

$$\left.\frac{\partial n}{\partial t}\right|_c = -\nu_k \left(n_1 - n_2\right)$$
$$\left.\frac{\partial nT}{\partial t}\right|_c = -\nu_k \left(n_1 T_1 - n_2 T_2\right) \tag{5.3}$$

where n_2 and $n_2 T_2$ are the moments of the reference Maxwellian (f_{M_0}) computed using the numerical quadrature scheme. Thus, for a case where the collision should identically vanish, we observe a violation of the particle and energy density conservation properties.

The above problem can be avoided with the help of an iterative process to define a Maxwellian (f_M) whose computed moments, n_2, T_2 do not deviate the computed moments of the distribution function n_1, T_1 beyond a given tolerance limit (say, $\epsilon \ll 1$)

$$\max\left(\left|\frac{n_2 - n_1}{n_1}\right|, \left|\frac{T_2 - T_1}{T_1}\right|\right) \le \epsilon$$

Due to the iterative nature of this procedure, and hence the multiple quadrature computations of the distribution functions, it is very expensive in practice.

5.3.1   Defining the reference Maxweliian

In the present work, we avoid the loss of conservation properties using a computationally less expensive alternative. We define the reference Maxwellian as a linear of combination of two Maxwellian distribution functions whose moments $n_{2_{a,\,b}}$, $T_{2_{a,\,b}}$ are such that

$$\min(T_{2_a}, T_{2_b}) \le T_1 \le \max(T_{2_a}, T_{2_b}) \tag{5.4}$$

$$\left| \frac{T_{2_b} - T_{2_a}}{T_1} \right| \leq \varepsilon \ll 1 \tag{5.5}$$

In a velocity grid of finite extent and fixed resolution, the numerical error in quadrature is influenced by the variance of the distribution function. Since temperature is the variance of the distribution function of a gas, the constraint is in terms of the temperatures of the Maxwellians.

The reference Maxwellian is of the form,

$$f_M(v) = \alpha_a f_{M_a}(v) + \alpha_b f_{M_b}(v) \tag{5.6}$$

where, denoting the weight of the ions by m_i,

$$n_{2_a} = \int d\vec{v} f_{M_a}(v) \qquad \& \qquad n_{2_a} T_{2_a} = \int d\vec{v} \frac{1}{3} m_i v^2 f_{M_a}(v)$$

$$n_{2_b} = \int d\vec{v} f_{M_b}(v) \qquad \& \qquad n_{2_b} T_{2_b} = \int d\vec{v} \frac{1}{3} m_i v^2 f_{M_b}(v) \tag{5.7}$$

For conservation of particle and energy density in the collision term, the moments of the reference Maxwellian must match that of the species distribution function

$$n_1 = \alpha_a n_{2_a} + \alpha_b n_{2_b}$$

$$n_1 T_1 = \alpha_a n_{2_a} T_{2_a} + \alpha_b n_{2_b} T_{2_b}$$

Solving for α_a & α_b in the above set of constraint, we obtain the final expression for the reference Maxwellian distribution function that conserves particle and energy densities,

$$f_M(v) = \frac{n_1}{n_{2_a}} \left(\frac{T_{2_b} - T_1}{T_{2_b} - T_{2_a}} \right) f_{M_a}(v) + \frac{n_1}{n_{2_b}} \left(\frac{T_1 - T_{2_a}}{T_{2_b} - T_{2_a}} \right) f_{M_b}(v) \tag{5.8}$$

The reference Maxwellian can be rewritten as,

$$f_M(v) = \frac{n_1}{n_{2_a}} \left(\frac{T_{2_b} - T_1}{T_{2_b} - T_{2_a}} \right) \left[f_{M_a}(v) + \frac{n_{2_a}}{n_{2_b}} \left(\frac{T_1 - T_{2_a}}{T_{2_b} - T_1} \right) f_{M_b}(v) \right] \tag{5.9}$$

In addition to satisfying the earlier constraint given by Eq. 5.4, we choose to define our f_{M_a} & f_{M_b} such that

$$\varepsilon_M = \left(\frac{T_1 - T_{2_a}}{T_1 - T_{2_b}} \right) \ll 1$$

For an adequately refined velocity grid, the numerical error is never comparable to the magnitudes of particle and energy densities. Hence, we always have,

$$\left| \frac{n_{2_b} - n_{2_a}}{n_{2_b}} \right| \ll 1$$

The reference Maxwellian expression is now in a form that deviates very little from that of of Gaussian distribution,

$$f_M(\mathrm{v}) = \frac{n_1}{n_{2_a}} \left(1 - \varepsilon_M\right) \left(f_{M_a}(\mathrm{v}) + \varepsilon_M \frac{n_{2_a}}{n_{2_b}} f_{M_b}(\mathrm{v}) \right) \tag{5.10}$$

Satisfying Eq. 5.4 ensures that the collision term always relaxes the distribution function to an approximately Maxwellian form. Defining reference Maxwellians, and their moments, is now done after regular time intervals to save on computation expense. In the following section, we test this collision model and present the results.

5.4   Numerical simulations

To test the performance of the Krook collision model (Eq.s 5.1 & 5.9), we consider plasma composed of ionized Hydrogen. We begin with an initial state that is described by Maxwellian distribution functions. We perturb the distribution function from this Maxwellian state and, after a finite duration of perturbation, then introduce the collisional relaxation, as computed by the Krook model. The simulation method can be described as,

$$\begin{aligned}
\frac{\partial f}{\partial t} &= \nu_p \frac{\mathcal{E}}{\mathcal{E}_m} \left(1 - \frac{\mathcal{E}}{\mathcal{E}_m}\right) f && \text{for } 0 \leq t \leq \tau_p \\
\frac{\partial f}{\partial t} &= -\nu_k \left(f - f_M\right) && \text{for } t \geq \tau_p
\end{aligned} \tag{5.11}$$

where $\mathcal{E}_m$ is the maximum energy in the $(\mathcal{E},\, \mu)$ velocity grid. The perturbation is maximum at a particle energy corresponding to the center of the velocity domain, and vanishes at the maximum $(\mathcal{E} = \mathcal{E}_m)$ and minumum $(\mathcal{E} = 0)$ energies. The perturbed plasma is described by a non–Maxwellian distribution function whose moments differ from the initial state. After a time τ_p the perturbation is switched off, and then the Krook collision operator is used to relax the distribution to a

Maxwellian state. For a particle and energy density conserving collision model, the zeroeth and second moments of the plasma distribution functin must remain constant during the collisional relaxation, and the distribution must relax to a Maxwellian.

$$\ln(f(v)\ v_{th}^3/n)$$
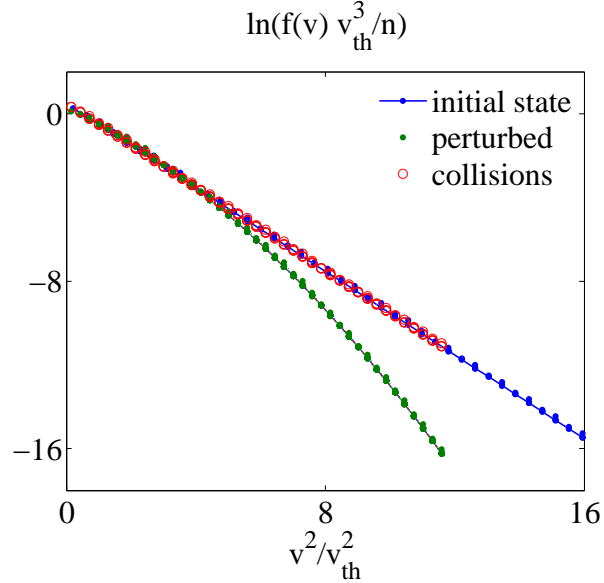
Figure 5.1: Collisional relaxation of a perturbed distribution function as computed using the Krook model (Eq.s 5.1 & 5.9).

In Fig. 5.1 we compare the perturbed distribution function with that of the initial and collisionally relaxed states. For a Maxwellian plasma distribution funtion, the logarithm of the distribution function, appropriately normalized by the local plasma density and thermal velocity $(v_{th}^3 f(v)/n)$, must vary linearly with energy normalized by temperature $(\mathcal{E}/T)$. We see that the distribution function is initially at a Maxwellian state, and the collisionally relaxed final state is of a Maxwellian form.

In Fig. 5.2 we compare the particle and energy densities of the perturbed plasma with the initial and collisionally relaxed states. As the perturbation is not of a form that conserves particle or energy densities, the perturbed plasma's particle and energy densities differ from the initial state. We see that the collisionally relaxed final state has the same particle and energy densities as the perturbed state while relaxing the distribution function to a Maxwellian form.
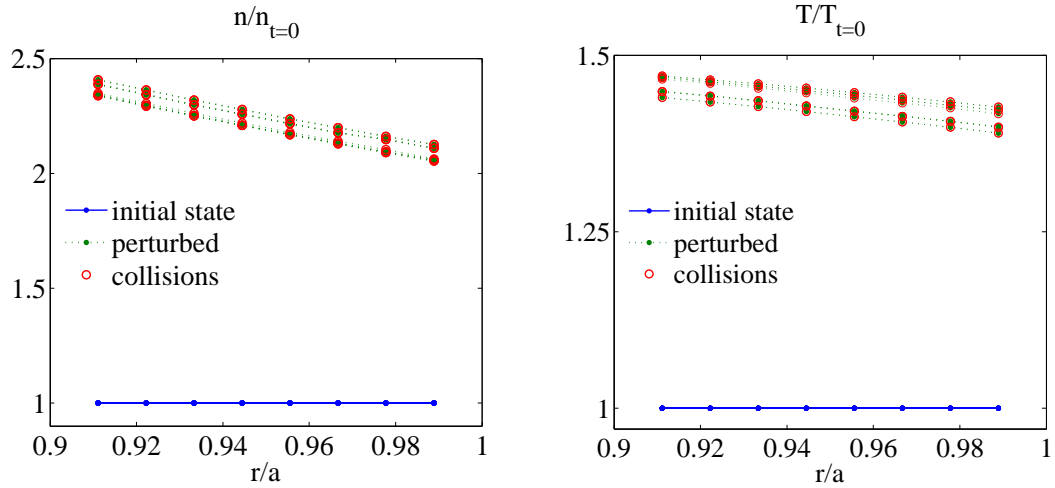
Figure 5.2: Evolution of particle and energy densities.

5.5   Summary

We have introduced the kinetic code TEMPEST for the simulation of toka-
mak edge plasmas. As a first step towards simulations to compute the transport
due to particle drifts, and plasma turbulence, we have presented the details of the
implementation of a particle and energy conserving Krook collision model. We
have tested the collision model by perturbing the distribution function and verify-
ing that the collision model relaxes the distribution function to a Maxwellian form
while conserving particle and energy density.

Chapter 5 contains material in preparation to be published as "Anomalous
radial transport model for kinetic codes", K. Bodi, R. H. Cohen, S. I. Krashenin-
nikov, T. D. Rognlien and X. Q. Xu. The dissertation author is the primary author
of this publication.

Chapter 6

Anomalous radial transport model for edge plasma

Anomalous transport, due to turbulent processes, is often the dominant part of the radial transport in edge plasma of magnetic confinement devices. Consequently any predictive simulation of edge plasma conditions requires the inclusion of anomalous radial transport. Since resolving the turbulence fully would require unreasonably long computation times, introducing a model for anomalous radial transport is a practicable approach. The coefficients/parameters of such a model can be defined using the knowledge gained from experiments and simulations that fully resolve turbuelnt motions. Towards this end, in this chapter we present a model for simulating anomalous radial transport in edge plasma for kinetic codes. We implement the model in the 4-D kinetic transport code TEMPEST, and present the results of the verification of the performance of the model.

6.1   Anomalous transport

In the kinetic description of plasmas, we consider the plasma to be the combination of its component species: electrons, various ions and various neutrals (if they exist). The evolution of each of the component species is described the

kinetic equation for its distribution function

$$\frac{\partial f}{\partial t} + \mathrm{v}_{||}\nabla_{||}f + \vec{\mathrm{v}}_{d_\perp} \cdot \vec{\nabla}_\perp f + E_{||}\frac{\partial f}{\partial \mathrm{v}_{||}} = S \qquad (6.1)$$

where s is the coordinate along the field–line, v_d is the particle drift velocity, $\mathrm{v}_{||}$ is the parallel velocity, and S is the source term that can also be modified to include the effects of collisions. As turbulent plasma is unsteady, rather than the instantaneous magnitudes, we are interested in the long–timescale averages of the various components of the kinetic equation. We can describe the the quantities (eg., f) as a combination of long–timescale averages (or mean quantities, $\langle f \rangle$) and fluctuations ($\tilde{f}$). Taking the long–timescale average of the kinetic equation (Eq. 6.1):

$$\frac{\partial \langle f \rangle}{\partial t} + \langle \mathrm{v}_{||}\nabla_{||}f \rangle + \langle \vec{\mathrm{v}}_{d_\perp} \cdot \vec{\nabla}_\perp f \rangle + \langle E_{||}\frac{\partial f}{\partial \mathrm{v}_{||}} \rangle = \langle S \rangle \qquad (6.2)$$

The nonlinear terms in the above equation have contributions from mean–quatities and fluctuations. For example, the advective term depending on the particle drift velocity becomes

$$\langle \vec{\mathrm{v}}_{d_\perp} \cdot \vec{\nabla}_\perp f \rangle = \langle \vec{\mathrm{v}}_{d_\perp} \rangle \cdot \vec{\nabla}_\perp \langle f \rangle + \langle \tilde{\vec{\mathrm{v}}}_{d_\perp} \cdot \vec{\nabla}_\perp \tilde{f} \rangle$$

For a transport code that intends to model the effect of terms like $\langle \tilde{\vec{\mathrm{v}}}_{d_\perp} \cdot \vec{\nabla}_\perp \tilde{f} \rangle$ without having to fully resolve the turbulence, the effect of such terms needs to be modelled. Modelling in such cases is effectively an expression relating the effect of unresolved terms ($\langle \tilde{\vec{\mathrm{v}}}_{d_\perp} \cdot \vec{\nabla}_\perp \tilde{f} \rangle$) in terms of the resolved quantities (like v_d, $\langle f \rangle$). The most common form of modelling turbulent transport is that of expressing it as a combination of advective transport that depends on the mean quantity, and a diffusive term that depends on the gradient of the mean quantity. Most predictive fluid transport codes, including those for edge transport, include such models for turbulent transport. In this chapter, we present such a model for kinetic codes. It should be noted that the assumption that the anomalous transport can be described accurately as a combination of advection and diffusion need not always be true for edge plasma where the correlation lengthscales of turbulence are comparable to the mean gradient lengthscales. However, in the absence of alternate models, it is the most economic model for anomalous transport calculations. In

this work, we only consider the radial component of anomalous transport since it directly affects the confinement of plasma.

6.2   Anomalous transport model

We model the anomalous radial flux ($\langle \tilde{v}_d \tilde{f} \rangle$) as a combination of advective and diffusive components. The advection and diffusion coefficient values are functions of velocity and spatial coordinates. The choice of the velocity dependence of the coefficients determines the form of the anomalous transport matrix in the fluid description. Considering only long–timescale averages (omitting the $\langle \rangle$ signs), we introduce a model for the radial component of the nonlinear term ($\langle \vec{\tilde{v}}_{d_\perp} \cdot \vec{\nabla}_\perp \tilde{f} \rangle$)

$$\frac{\partial f}{\partial t} + v_{||} \nabla_{||} f + \vec{v}_{d_\perp} \cdot \vec{\nabla}_\perp f + E_{||} \frac{\partial f}{\partial v_{||}} + \vec{\nabla}_\psi \cdot [\Gamma_a \hat{e}_\psi]_{\theta, \vec{v}} = S \tag{6.3}$$

where $\hat{e}_\psi$ is the unit vector normal to the flux–surface, and the anomalous radial flux (Γ_a) is defined as

$$\Gamma_a = U_a(\psi, \hat{v}) f - D_a(\psi, \hat{v}) \left. \nabla_\psi f \right|_{\theta, \vec{v}} \tag{6.4}$$

Here, $\hat{v} = v/v_{th}$ is the velocity normalized by the local ion thermal velocity ($v_{th} = \sqrt{2T/m}$). For non–uniform temperature, $\hat{v}$ is spatially non–uniform. The velocity space in most kinetic codes are defined to take advantage of conserved quantities like $\mathcal{E}$, and adiabatic invariant, μ. Typically velocity grids are expressed as a $(\mathcal{E}, \mu)$ grid, or a $(\mathcal{E}, v_{||}/v)$ grid, where $\mathcal{E} = mv^2/2 + q\Phi$ is the energy of the charged particles, $\mu = mv_\perp^2/2B$ is the magnetic moment, and $v_{||}/v$ represents the pitch–angle. Thus the 3–D velocity space is approximated by a 2–D grid. In such descriptions, since the velocity grid is affected by spatially varying fields (the electrostatic potential Φ and magnetic field B), care should be taken that derivatives are taken along contours of fixed velocity vectors. Equations 6.3 & 6.4 reflect this constraint. For an $(\mathcal{E}, \mu)$ velocity grid, like that used in TEMPEST, the gradients along contours of constant $\vec{v}$ is computed as

$$\left. \nabla_\psi f \right|_{\vec{v}} = \frac{\partial f}{\partial \psi} + q \frac{\partial \Phi}{\partial \psi} \frac{\partial f}{\partial \mathcal{E}} - \frac{\mu}{B} \frac{\partial B}{\partial \psi} \frac{\partial f}{\partial \mu} \tag{6.5}$$

The above directional derivative can also be computed as a finite difference of distribution function whose values along the constant velocity ($\mathcal{E} - q\Phi(\psi) = $ const., $\mu B(\psi) = $ const.) contour can be computed using an interpolation scheme. In the present work, we consider plasma in closed field–line region with slowly varying magnetic fields and with no electrostatic fields ($|\nabla\Phi| = 0$) and hence, we evaluate the directional derivatives using Eq. 6.5 in the simulations shown here.

Transport Coefficients

In Eq. 6.4, we had approximated the anomalous flux in the form of convective and diffusive components that depend on the coefficients $U_a(\psi, \hat{v})$ and $D_a(\psi, \hat{v})$ respectively. The form of these coefficients determines the fluid transport matrix. For example, for Maxwellian distribution functions, $U_a = 0$ & $D_a = D_0$ describe a diagonal fluid transport matrix with equal diffusivities for fluid density and temperature. We can obtain indpendent control over the global transport matrix by appropriately choosing the velocity dependence of the coefficients, U_a & D_a. In this process, considerations of numerical stability requre that the diffusion coefficient, $D_a(\psi, \hat{v})$, be non–negative.

For numerical stability, the diffusion coefficient is required to be positive. This constraint arises from the nature of the diffusion operator. A positive diffusion coefficient is one that flattens fluctuations. It follows that the effect of a negative diffusion coefficient is the sharpening of fluctuations. In a computation involving dispersion errors due to the differencing scheme, a negative diffusion coefficient will lead to growth in fluctuations due to errors and hence, numerical instability. For this reason, our diffusion coefficient needs to be positive at all velocity and spatial coordinates.

Determining the coefficient values

To compare the transport matrix due to our anomalous transport model with equivalent models for fluid codes, we need to consider the moments of the anomalous flux (Eq. 6.4). We make the comparison for the case of a plasma

described by a Maxwellian distribution function, which is the case for a fluid in thermodynamic equilibrium. The particle and heat fluxes due to the anomalous flux are of the form,

$$\Gamma_n = \int d\vec{v}\,\Gamma_a \quad = \int d\vec{v}\,\left[U_a(\psi,\hat{v})f - D_a(\psi,\hat{v})\,\nabla_\psi f|_{\theta,\vec{v}}\right]$$

$$Q = \int d\vec{v}\,\frac{1}{2}mv^2\Gamma_a = \int d\vec{v}\,\frac{1}{2}mv^2\left[U_a(\psi,\hat{v})f - D_a(\psi,\hat{v})\,\nabla_\psi f|_{\theta,\vec{v}}\right] \qquad (6.6)$$

A velocity dependent convective coefficient would lead to a polynomial in terms of density, n, and temperature, T. For a simple, velocity–independent, convective coefficient the general form of the fluxes would then be,

$$\Gamma_n = U_1(\psi)n - D_{11}\nabla_\psi n - D_{12}n\frac{1}{T}\nabla_\psi T$$

$$Q = U_2(\psi)nT - D_{21}T\nabla_\psi n - D_{22}n\nabla_\psi T \qquad (6.7)$$

where U_1 & U_2 are the convective coefficients, and D_{11}, D_{12}, D_{21} & D_{22} are the coefficients for gradient driven transport.

Typically, long–time average transport due to turbulence is modelled as dependent on gradients of long–time averages of density and temperature of the fluid. Anomalous flux, in such models, is of a purely diffusive nature. Here, we demonstrate how the tranpsort model in equations 6.3 & 6.4 can include such models.

The transport matrix, for anomalous particle and heat fluxes that dependent only on the gradients of density and temperature, is of the form

$$-\Gamma_n = D_{11}\nabla_\psi n + D_{12}n\frac{1}{T}\nabla_\psi T$$

$$-Q = D_{21}T\nabla_\psi n + D_{22}n\nabla_\psi T \qquad (6.8)$$

For an anomalous flux of the form of Eq. 6.4, a velocity dependence for the diffusive coefficient $(D_a(\psi,\hat{v}))$ of form of a polynomial in $\hat{v} = v/v_{th}$ results in terms that are proportional to gradients in density and temperature. For the contribution from the convective term to be of a similar form, the convective coefficient must be dependent on the gradient length–scales of density and temperature,

$$U_a(\psi,\hat{v}) \equiv U_a(\psi) = D_\alpha(\psi)\frac{1}{n}\nabla_\psi n + D_\beta(\psi)\frac{1}{T}\nabla_\psi T \qquad (6.9)$$

where the coefficients D_α & D_β have the same units as the diffusion coefficient D_a. Our anomalous flux is of the form,

$$\Gamma_a = \left[D_\alpha \frac{1}{n} \nabla_\psi n + D_\beta \frac{1}{T} \nabla_\psi T \right] f - D_a(\psi, \hat{v}) \left. \nabla_\psi f \right|_{\theta, \vec{v}} \tag{6.10}$$

In this work we consider the case of D_a being a polynomial in $\hat{v}$. Since our reference case is that corresponding to a Maxwellian, for convenience in moment computation, we express the polynomial form as a combination of Hermite polynomials of successive orders,

$$D_a(\psi, \hat{v}) = D_0(\psi) + D_2(\psi) \left(\frac{v^2}{v_{th}^2} - \frac{1}{2} \right) + D_4(\psi) \left(\frac{v^4}{v_{th}^4} - 3\frac{v^2}{v_{th}^2} + \frac{3}{4} \right) \tag{6.11}$$

It should be noted that, beyond the explicit spatial dependence of the coefficients, D_0, D_2 & D_4, there is also an implicit spatial dependence in the $\hat{v}$ terms, through the dependence of $\hat{v}$ on temperature and electrostatic potential,

$$\hat{v} = \frac{v}{v_{th}} = \sqrt{\frac{\mathcal{E} - q\Phi(\psi)}{T(\psi)}}$$

For computing the transport matrix, we consider the distribution function to be a Maxwellian,

$$f_M(\vec{v}) = \frac{n}{(\sqrt{\pi} v_{th})^3} \exp\left(-\frac{v^2}{v_{th}^2} \right)$$

To compute the moments of the anomalous, we take advantage of the following relation for the moments of a Maxwellian,

$$\int d\vec{v} \left(\frac{1}{2} m v^2 \right)^r f_M(\vec{v}) = \left[\prod_{s=0}^{r} \left(\frac{2s+1}{2} \right) \right] 2nT^r \tag{6.12}$$

While computing the moments (Eq. 6.6), one should note that the thermal velocity need not be spatially uniform. Thus, contributions from the diffusive component

of the flux are of the form,

$$
\int d\vec{\mathrm{v}} \left(\frac{\mathrm{v}^2}{\mathrm{v}_{th}^2}\right)^r \nabla_\psi f(\vec{\mathrm{v}})|_{\theta,\vec{\mathrm{v}}} = \int d\vec{\mathrm{v}} \frac{1}{T^r} \left(\frac{1}{2}m\mathrm{v}^2\right)^r \nabla_\psi f(\vec{\mathrm{v}})|_{\theta,\vec{\mathrm{v}}}
$$

$$
= \int d\vec{\mathrm{v}} \frac{1}{T^r} \nabla_\psi \left[\left(\frac{1}{2}m\mathrm{v}^2\right)^r f(\vec{\mathrm{v}})\right]_{\theta,\vec{\mathrm{v}}}
$$

$$
= \frac{1}{T^r} \nabla_\psi \left[\int d\vec{\mathrm{v}} \left(\frac{1}{2}m\mathrm{v}^2\right)^r f(\vec{\mathrm{v}})\right]_\theta \qquad (6.13)
$$

For a Maxwellian distribution function, we thus have,

$$
\int d\vec{\mathrm{v}} \left(\frac{\mathrm{v}^2}{\mathrm{v}_{th}^2}\right)^r \nabla_\psi f_M(\vec{\mathrm{v}})|_{\theta,\vec{\mathrm{v}}} = \frac{1}{T^r} \nabla_\psi \left[\left(\prod_{s=0}^{r} \left(\frac{2s+1}{2}\right)\right) 2nT^r\right]_\theta
$$

$$
= 2 \left(\prod_{s=0}^{r} \left(\frac{2s+1}{2}\right)\right) \left[\nabla_\psi n + r\frac{1}{T}\nabla_\psi T\right] \qquad (6.14)
$$

The anomalous transport matrix (Eq. 6.6), for the above form of U_a (Eq. 6.9) and D_a (Eq. 6.11), using Eq. 6.14, is

$$
-\Gamma_n = [D_0 + D_2 - D_\alpha]\nabla_\psi n + \frac{3}{2}\left[D_2 + 2D_4 - \frac{2}{3}D_\beta\right]n\frac{1}{T}\nabla_\psi T
$$

$$
-Q = \frac{3}{2}[D_0 + 2D_2 + 2D_4 - D_\alpha]T\nabla_\psi n + \frac{3}{2}\left[D_0 + \frac{9}{2}D_2 + 12D_4 - D_\beta\right]n\nabla_\psi T
$$

$$
\qquad (6.15)
$$

Matching it with a desired transport matrix, Eq. 6.8, requires the meeting of the constraints,

$$
\begin{bmatrix} -1 & 0 & 1 & 1 & 0 \\ 0 & -\frac{2}{3} & 0 & 1 & 2 \\ -1 & 0 & 1 & 2 & 2 \\ 0 & -1 & 1 & \frac{9}{2} & 12 \end{bmatrix} \cdot \begin{Bmatrix} D_\alpha \\ D_\beta \\ D_0 \\ D_2 \\ D_4 \end{Bmatrix} = \begin{Bmatrix} D_{11} \\ \frac{2}{3}D_{12} \\ \frac{2}{3}D_{21} \\ \frac{2}{3}D_{22} \end{Bmatrix} \qquad (6.16)
$$

We have to meet four constraints involving five parameters. This gives us the additional flexibility that is required in order to meet to the additional constraint of positivity of the diffusion coefficient over the entire domain,

$$
D_a = D_0(\psi) + D_2(\psi)\left(\frac{\mathrm{v}^2}{\mathrm{v}_{th}^2} - \frac{1}{2}\right) + D_4(\psi)\left(\frac{\mathrm{v}^4}{\mathrm{v}_{th}^4} - 3\frac{\mathrm{v}^2}{\mathrm{v}_{th}^2} + \frac{3}{4}\right) \geq 0 \qquad (6.17)
$$

6.2.1 Illustration: Diagonal Transport Matrix

To illustrate the ability of the anomalous transport matrix to match a desired fluid transport matrix, we consider the case of a diagonal transport matrix similar to that of transport in a typical conducting fluid. Such a fluid is typically defined by its Diffusivity (D_n) that determines the particle diffusion rate, Conductivity (χ) that determines the heat conduction rate, and Specific Heat (C_p) that determines the convective heat transfer. The transport matrix for such a fluid is,

$$-\Gamma_n = D_n \nabla_\psi n$$
$$-Q = \frac{5}{2} T D_n \nabla_\psi n + \chi n \nabla_\psi T \tag{6.18}$$

We can see that the particle flux is driven solely by the density gradient in this case. A comparison with the transport matrix described by our model leads to the following constraints

$$D_n = D_0 + D_2 - D_\alpha \tag{6.19a}$$

$$0 = D_2 + 2D_4 - \frac{2}{3} D_\beta \tag{6.19b}$$

$$\frac{5}{3} D_n = D_0 + 2D_2 + 2D_4 - D_\alpha \tag{6.19c}$$

$$\frac{2}{3} \chi = D_0 + \frac{9}{2} D_2 + 12 D_4 - D_\beta \tag{6.19d}$$

Equations 6.19a–6.19c lead to the condition

$$D_\beta = D_n \tag{6.20}$$

Eq.s 6.19a, 6.19b, 6.19d & 6.20 lead to

$$D_4 = \frac{1}{5} \left[\frac{2}{3} \left(\chi - \frac{7}{2} D_n \right) - D_\alpha \right] \tag{6.21}$$

and hence,

$$D_2 = \frac{2}{3} D_n - 2 D_4$$
$$D_0 = D_n - D_2 + D_\alpha \tag{6.22}$$

Thus, our choice of D_α determines the form of the convective (U_a) and diffusive (D_a) coefficients. For a simple quadratic dependence of the diffusive coefficient over the velocity, we set

$$D_\alpha = \frac{2}{3}\left(\chi - \frac{7}{2}D_n\right) \tag{6.23}$$

leading to

$$D_4 = 0$$
$$D_2 = \frac{2}{3}D_n$$
$$D_0 = \frac{1}{3}D_n + D_\alpha \tag{6.24}$$

The convective and diffusive coefficients are of the form

$$U_a = \frac{2}{3}\left(\chi - \frac{7}{2}D_n\right)\frac{1}{n}\nabla_\psi n + D_n\frac{1}{T}\nabla_\psi T \tag{6.25a}$$

$$D_a = \frac{2}{3}\left(\chi - \frac{7}{2}D_n\right) + \frac{2}{3}D_n\hat{v}^2 \tag{6.25b}$$

These coefficients in the anomalous flux (Eq. 6.4) result in the fluid transport matrix given by Eq. 6.18 for species obeying a Maxwellian distribution function. As to the constraint about the positivity of the diffusive coefficient, we can see, from Eq. 6.25b, that the condition now is

$$D_\alpha = \frac{2}{3}\left(\chi - \frac{7}{2}D_n\right) \geq 0 \tag{6.26}$$

6.3 Verification of the transport model

To verify the anomalous transport model, we consider a modified kinetic equation that does not have the effects of particle drifts and accelerations. This modified kinetic equation is of the form

$$\frac{\partial f}{\partial t} + \vec{\nabla}_\psi \cdot [\Gamma_a \hat{e}_\psi]_{\theta,\vec{v}} = 0 \tag{6.27}$$

We consider test–cases corresponding to two different transport matrices. The domain of interest in these computations is an annulus in a tokamak. Since the goal of our present investigation is the verification of the ability of our transport
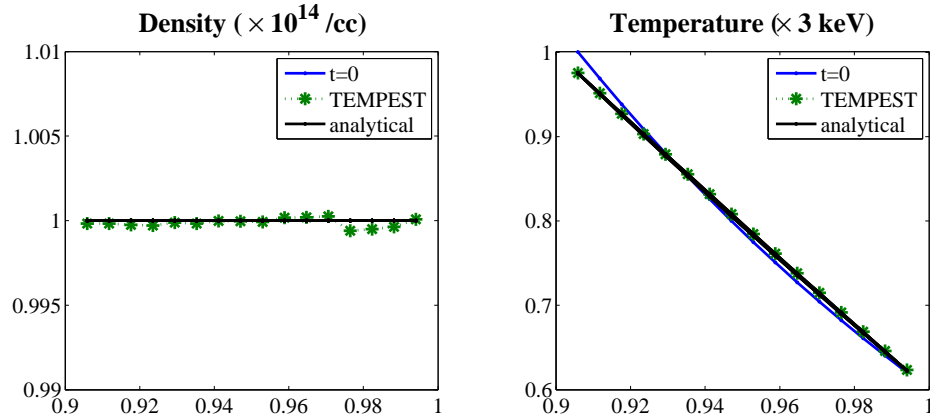
Figure 6.1: Steady–state solution for anomalous transport model (Eq. 6.28) in TEMPEST compared with the solution for the equivalent fluid model (Eq. 6.29)

model to match equivalent models in fluid codes, we consider the simple case of close field–lines. To illustrate the performance of the model, we consider different forms of the anomalous transport model, and verify that the resulting steady–state solution from the kinetic simulation matches that of the transport matrix that they are designed to match. The latter are the solutions of ordinary differential equations corresponding to the divergence of fluid–fluxes set to zero.

6.3.1 $U_a = 0$, $D_a(\hat{\mathbf{v}}) = D_n$

For a uniform diffusivity for all velocities, in the absence of an advective component, the anomalous radial flux is of the form,

$$\Gamma_a = -D_n \, \nabla_\psi f|_{\vec{\mathbf{v}}} \tag{6.28}$$

We can see, from Eq. 6.15, that for a purely diffusive anomalous flux with a constant diffusive coefficient (D_a) for all velocities, the fluid transport matrix is of the form

$$-\Gamma_n = D_n \nabla_\psi n$$
$$-Q = \frac{3}{2} D_n T \nabla_\psi n + \frac{3}{2} D_n n \nabla_\psi T \tag{6.29}$$

For a transport model defined by a single parameter, D_n, clearly, we can only
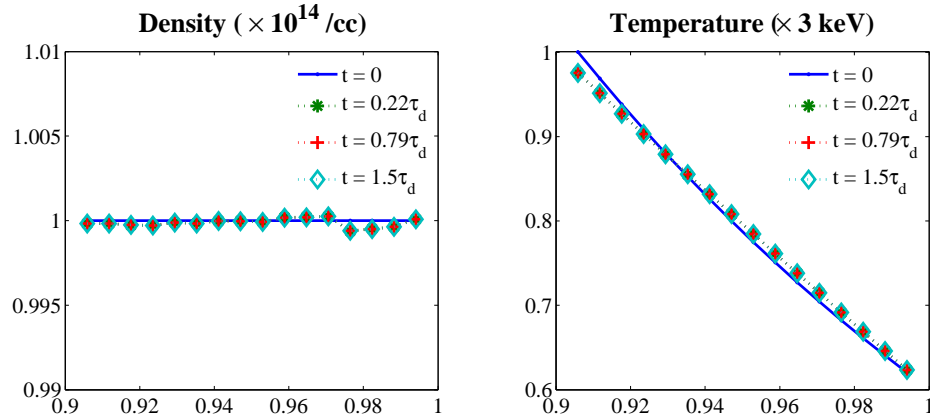
Figure 6.2: Evolution of flux–averaged density and temperature for Eq. 6.28 follows the physical picture for Eq. 6.29 of density remaining uniform. Density deviation from uniformity can be seen to be much smaller than 1%.

have one independent parameter in such a tranport matrix. The conductivity in the above matrix is defined as a multiple of diffusivity, $\chi = 1.5 D_n$.

For a plasma with uniform density, our problem is that of heat conduction. So the steady–state solution is that of heat conduction problem in an annulus, with particle density remaining uniform across the domain. From the results of a simulation run with these conditions, as shown in Fig. 6.1, we can see that our transport model matches the result of our physical intuition. Plotted in the figure are the flux–surface averaged values of ion density and temperature. We expect the density to remain uniform during the simulation, and we see that in Fig. 6.2 that the ion density remains almost uniform, with the deviation from uniformity remaining much smaller than 1%.

6.3.2 $\quad U_a = D_\beta \nabla_\psi \ln T, \; D(\hat{\mathbf{v}}) = D_2 \hat{\mathbf{v}}^2$

We now choose a model with a diffusive coefficient that is a quadratic polynomial in $\hat{\mathbf{v}}$. In order to obtain a diagonal transport matrix, we choose a suitable advective coefficient. Comparing the diffusive coefficient with Eq. 6.24, we see that $D_\alpha = 0$ and $D_\beta = D_n$. Thus the anomalous radial flux is of the form,

$$\Gamma_a = D_n \frac{1}{T} \nabla_\psi T f - \frac{2}{3} D_n \hat{\mathbf{v}}^2 \; \nabla_\psi f |_{\vec{\mathbf{v}}} \tag{6.30}$$

Figure 6.3: Steady–state solution for anomalous transport model (Eq. 6.30) in TEMPEST compared with the solution for the equivalent fluid model (Eq. 6.31)

We can see, from Eq. 6.15, that for the above form of anomalous flux, the fluid transport matrix is of the form

$$-\Gamma_n = D_n \nabla_\psi n$$
$$-Q = \frac{5}{2} D_n T \nabla_\psi n + \frac{7}{2} D_n n \nabla_\psi T \qquad (6.31)$$

The transport matrix is, once again, defined by only one independent parameter.

Figure 6.4: Evolution of flux–averaged density and temperature for Eq. 6.30 follows the physical picture for Eq. 6.31 obtained from the magnitudes of coefficients. Temperature evolution is faster than the density evolution.

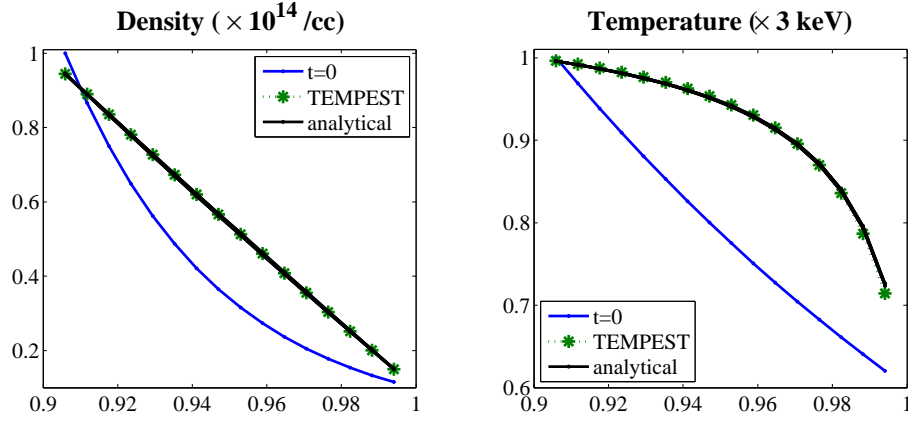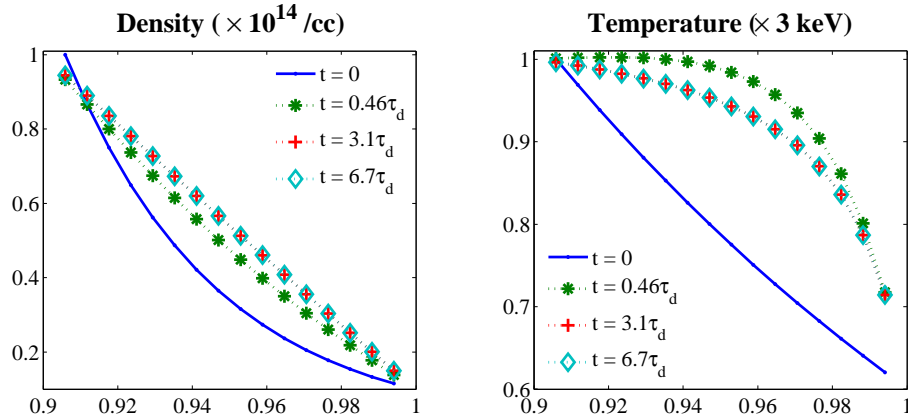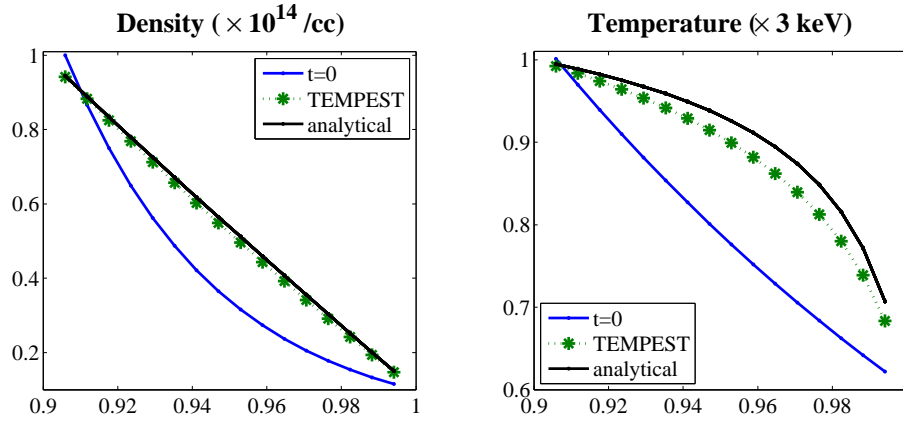**Density ($\times 10^{14}$ /cc)**   **Temperature ($\times$ 3 keV)**

Figure 6.5: Steady–state solution for anomalous transport model (Eq. 6.32) in TEMPEST compared with the solution for the equivalent fluid model (Eq. 6.33) for $D_n = 10$ & $\chi = 50 m^2/s$

The conductivity is related to the diffusivity as $\chi = 3.5 D_n$. The solution of the density conservation equation in this case is that of the divergence of particle flux is zero. For a circular annulus, the solution is that of a logarithmic profile. Since our domain width is only 10% of the radius of the annulus, the profile is very close to a linear variation. We see that the steady–state density profile in Fig. 6.3 matches this expectation. From the evolution plot in Fig. 6.4, we see that the temperature evolution is faster than that of the density, as one expects from the fact that $\chi = 3.5 D_n$, and since convective transport is non–negligible, steady–state for the temperature profile is reached only along with that of particle density.

6.3.3 $U_a = D_\alpha \nabla_\psi \ln n + D_\beta \nabla_\psi \ln T, \; D(\hat{\mathbf{v}}) = D_0 + D_2 \hat{\mathbf{v}}^2$

We now choose a model with a convective coefficient that depends on gradients of energy as well as particle density. Thus the anomalous radial flux is,

$$\Gamma_a = \left[\frac{2}{3} \left(\chi - \frac{7}{2} D_n \right) \; \frac{1}{n} \nabla_\psi n + D_n \; \frac{1}{T} \nabla_\psi T \right] f$$
$$- \left[\frac{2}{3} \left(\chi - \frac{7}{2} D_n \right) + \frac{2}{3} D_n \hat{v}^2 \right] \nabla_\psi f |_{\vec{v}} \quad (6.32)$$

We can see, from Eq. 6.15, that for the above form of anomalous flux, the fluid

ln(f(v) v³_th/n)
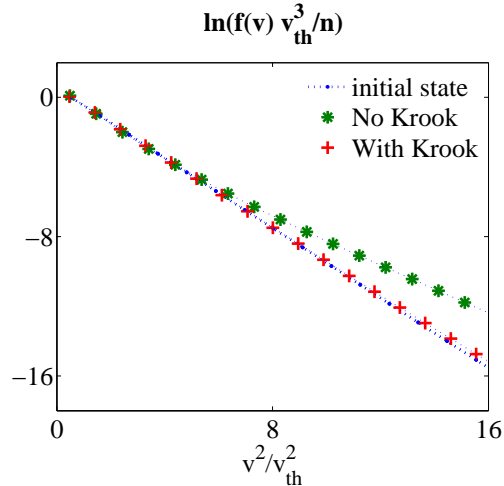
Figure 6.6: Distribution function deviates from a Maxwellian states under the influence of the anomalous transport opertor. Introducing the Krook collision model remedies this effect.

transport matrix is of the form

$$-\Gamma_n = D_n \nabla_\psi n$$

$$-Q = \frac{5}{2} D_n T \nabla_\psi n + \chi n \nabla_\psi T \tag{6.33}$$

To test the performance of our model, we consider a plasma whose conductivity is $\chi = 50\text{m}^2/\text{s}$, and diffusivity is $D_n = 10\text{m}^2/\text{s}$. For this test, we consider the case of a uniform magnetic field. The steady–state solution, as shown in Fig. 6.5, does not match with the analytical solution that we expect. Since the analytical solution is for the case of a Maxwellian distribution function, we first verify the form of the distribution function. Fig. 6.6 shows the distribution function at one particular radial location. We can see that the distribution function, as evolved by the anomalous transport model, is not in the form of a Maxwellian. The transport model, due to its quadratic dependence on velocity, distorts the tail of the distribution. To retain the Maxwellian nature of the distribution function, we have added a particle and energy conserving Krook collision model (Sec. 5.2). The steady–state solution attained by the anomalous transport model, in the presence of Krook collision model, is shown in Fig. 6.7. From Fig. 6.7, we can clearly see that the collisional relaxation of the distribution function towards a Maxwellian
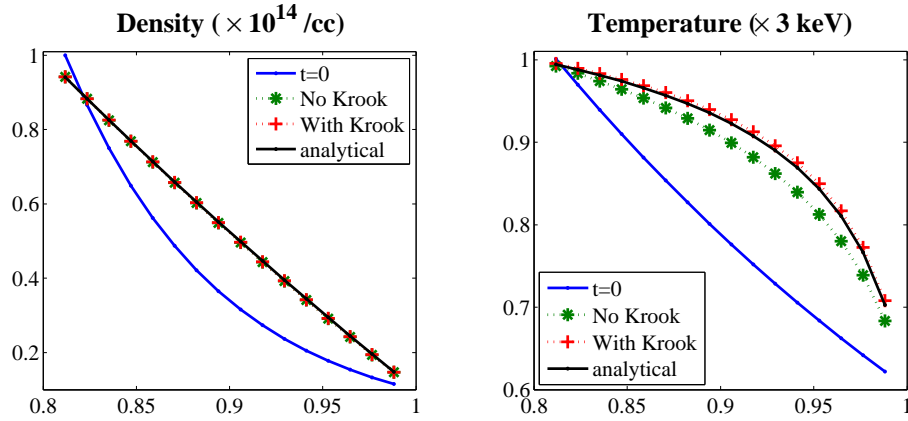
Figure 6.7: Effect of introducing the Krook collision operator on the steady–state solution for anomalous transport model (Eq. 6.32) in TEMPEST. Comparison is done, as in Fig. 6.5 with the solution for the equivalent fluid model (Eq. 6.33) for $D_n = 10$ & $\chi = 50 m^2/s$

form results in better agreement of the steady–state reached by the anomalous transport model in TEMPEST with analytical expectation.

Conducting but non–diffusive plasma

To test the performance of our model, we consider a conducting, but not diffusive, plasma. This corresponds to $D_n = 0$ and $\chi \neq 0$.

$$-\Gamma_n = 0$$
$$-Q = \chi n \nabla_\psi T \qquad (6.34)$$

For this test, we consider the case of a uniform magnetic field. As can be seen in Eq. 6.34, the particle flux vanishes for $D_n = 0$ and, the equation for the evolution of particle density reduces to the trivial case of density remaining constant. The energy flux is dependent only on the conductivity, and the solution of the energy conservation equation in this case is that of the divergence of energy flux is zero. We compare the steady–state profiles of particle and energy density to the expected values from the transport matrix in Fig. 6.8, and we show the time evolution in Fig. 6.9. We can see that the density profile remains unchanged while the temperature profile matches this expected profile.
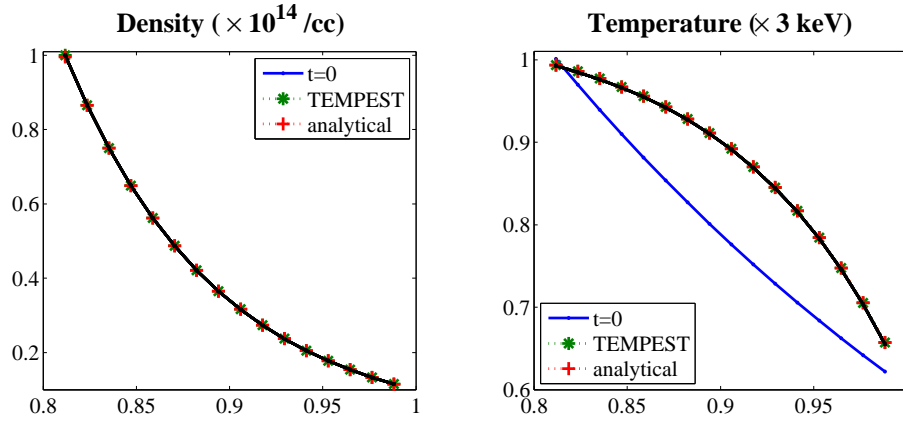
Figure 6.8: Steady–state solution for anomalous transport model (Eq. 6.32) in TEMPEST compared with the solution for the equivalent fluid model (Eq. 6.34) for $D_n = 0$ & $\chi = 50m^2/s$

6.4 Summary

In this work we have presented a model to simulate anomalous radial transport in the edge plasma using kinetic codes. In this model we represent the anomalous transport as a combination of convective and diffusive transport whose coefficients can be obtained from experimental observations, or from simulations of edge turbulence. We have implemented the model in the 4–D version of the kinetic code TEMPEST. We have verified the performance of the model by comparing its results for the case of gradient driven transport to analytical expectations in the closed field–line region of tokamak edge plasma.

Chapter 6 contains material in preparation to be published as "Anomalous radial transport model for kinetic codes", K. Bodi, R. H. Cohen, S. I. Krasheninnikov, T. D. Rognlien and X. Q. Xu. The dissertation author is the primary author of this publication. The text of chapter 6 contains material of the paper "TEMPEST simulations of the plasma transport in a single-null tokamak geometry", X. Q. Xu, K. Bodi, R. H. Cohen, S. Krasheninnikov and T. D. Rognlien, in communication to be published in Nuclear Fusion. The dissertation author is a contributing author of this publication.

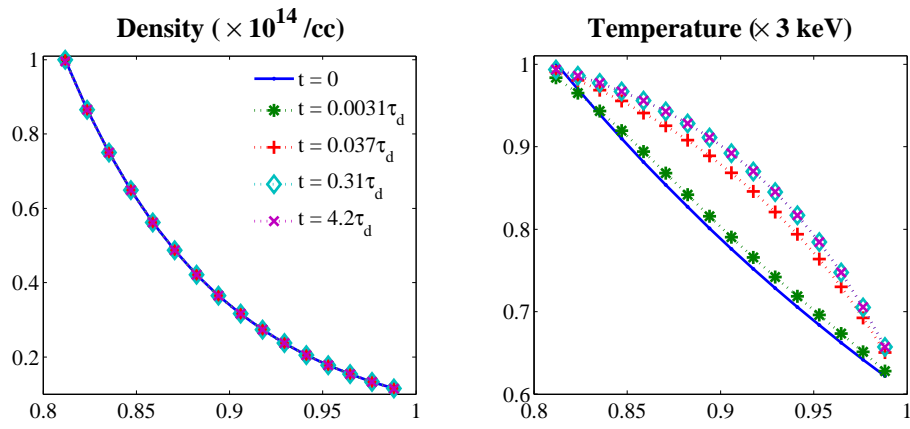Figure 6.9: Evolution of flux–averaged density and temperature for Eq. 6.32 follows the physical picture for Eq. 6.34 obtained from the magnitudes of coefficients.

Chapter 7

Summary and Conclusions

In this thesis we have presented the results of our studies on anomalous radial transport in tokamak edge plasma. Contributions of the present thesis can be divided into two areas: intermittent convective transport (*blobs*) in edge plasma, and *anomalous transport model* for kinetic codes simulating edge plasma. In chapters 2–4 we present our work on the mechanism of generation and propagation of blobs in edge plasma. In chapters 5 & 6 we present our work on the simulation of edge plasma using kinetic codes.

In chapter 2 we have discussed the mechanism of generation of coherent mesoscale structures that constitute the anomalous radial transport in edge plasma. Using the technique of four–wave interactions we have considered the stability of mesoscale electromagnetic structures in the presence of interchange drive and electrostatic drift–wave turbulence, and have shown that smallscale electrostatic (drift–wave) turbulence may generate filamentary (elongated along fieldlines) mesoscale electromagnetic structures (*blobs*).

In chapter 3 we have presented numerical simulations that were performed to verify the formation of mesoscale structures as a result of smallscale electrostatic drift–wave turbulence. We considered the interaction of drift–wave turbulence, interchange drive and fieldline–tension in a 2–D domain in the closed fieldline region of the outer midplane of the tokamak edge. We have shown that, even for edge plasma gradients where interchange drive is stabilized by fieldline tension, drift–wave turbulence results in the formation of mesoscale structures like blobs.

In chapter 4 we have presented our study on the effect of edge plasma gradients on the propagation of blobs. Based on the conservation of the total kinetic energy of the convecting blob and the flow–field in the surrounding (that depends on the plasma density), we first argued that blobs convecting towards regions of lower density accelerate. Similarly holes (blobs with lower density than surrounding plasma) convecting towards the core must decelerate. We have presented numerical simulations whose results confirm the preferential propagation of blobs into regions of low plasma density. Since the kinetic energy depends on the local plasma density, this effect is lost in analyses that use the Boussinesque approximation in the vorticity equation.

In chapter 5 we introduced the 5–D kinetic code TEMPEST for simulating tokamak edge plasma. In its 4–D form TEMPEST can be run as a kinetic transport code for the edge. In order to compute neoclassical transport due to particle drifts TEMPEST needs a collision model. As a first step we have added a Krook collision model that conserves particle and energy densities. We have presented the formulation and implementation of the model, and have demonstrated that it can restore a perturbed distribution function to a Maxwellian form while conserving the particle and energy densities.

Intermittent coherent structures (*blobs*) that have been discussed in chapters 2, 3 & 4 are a feature of anomalous transport in edge plasma. In chapter 6 we have presented the formulation of a model for anomalous transport in kinetic codes. The model is capable of representing convective and diffusive fluxes. We have presented the details of implementation of the model for TEMPEST. In order to demonstrate the flexibility of our anomalous transport model we have tested its performance in the closed fieldline region for different transport matrices and showed that the results match analytical expectations. Since TEMPEST is capable of handling the scrape–off layer, our anomalous transport model can be extended to the scrape–off layer. Particle and heat fluxes to the chamber wall are of interest in relation to the issues of erosion of chamber walls, impurities and even confinement. Computations using the anomalous transport model in the edge scrape–off layer can help improve our understanding in this area.

Bibliography

[1] B. B. Kadomtsev. *Tokamak plasma: a complex physical system.* IOP Publishing Ltd, 1992.

[2] J. Wesson. *Tokamaks.* Oxford University Press, 2004.

[3] A. A. Galeev and R. Z. Sagdeev. Transport phenomena in rarefield plasma in toroidal magnetic traps. *Sov. Phys. JETP*, 53:233, 1968.

[4] F. L. Hinton and R. D. Hazeltine. Theory of plasma transport in toroidal confinement systems. *Reviews of Modern Physics*, 48(2):239–308, 1976.

[5] M. V. Umansky, S. I. Krasheninnikov, B. LaBombard, and J. L. Terry. Comments on particle and energy balance in the edge plasma of alcator c-mod. *Physics of Plasmas*, 5(9):3373–3376, 1998. doi: 10.1063/1.873051. URL `http://link.aip.org/link/?PHP/5/3373/1`.

[6] S. I. Krasheninnikov. On scrape-off layer plasma transport. *Physics Letters, Section A: General, Atomic and Solid State Physics*, 283(5-6):368–370, 2001.

[7] G. Q. Yu. *Non-diffusive Cross Field Transport in Scrape-off-Layer in Tokamak.* PhD thesis, University of California, San Digeo, 2006.

[8] S. I. Krasheninnikov, D. A. D'Ippolito, and J. R. Myra. Recent theoretical progress in understanding coherent structures in edge and sol turbulence. *Journal of Plasma Physics*, 74(5):679–717, 2008.

[9] X. Q. Xu, Z. Xiong, M. R. Dorr, J. A. Hittinger, K. Bodi, J. Candy, B. I. Cohen, R. H. Cohen, P. Colella, G. D. Kerbel, S. Krasheninnikov, W. M.

Nevins, H. Qin, T. D. Rognlien, P. B. Snyder, and M. V. Umansky. Edge gyrokinetic theory and continuum simulations. *Nuclear Fusion*, 47(8):809–816, 2007.

[10] R. H. Cohen and X. Q. Xu. Progress in kinetic simulation of edge plasmas. *Contributions to Plasma Physics*, 48:212–223, 2007.

[11] D. H. J. Goodall. High speed cinefilm studies of plasma behaviour and plasma surface interactions in tokamaks. *Journal of Nuclear Materials*, 111-112(C): 11–22, 1982.

[12] S. J. Zweben. Search for coherent structure with in tokamak plasma turbulence. *Physics of Fluids*, 28(3):974–982, 1985.

[13] J. A. Boedo, D. Rudakov, R. Moyer, S. Krasheninnikov, D. Whyte, G. McKee, G. Tynan, M. Schaffer, P. Stangeby, P. West, S. Allen, T. Evans, R. Fonck, E. Hollmann, A. Leonard, A. Mahdavi, G. Porter, M. Tillack, and G. Antar. Transport by intermittent convection in the boundary of the diii-d tokamak. *Physics of Plasmas*, 8(11):4826–4833, 2001.

[14] J. L. Terry, R. Maqueda, C. S. Pitcher, S. J. Zweben, B. Labombard, E. S. Marmar, A. Yu. Pigarov, and G. Wurden. Visible imaging of turbulence in the sol of the alcator c-mod tokamak. *Journal of Nuclear Materials*, 290-293: 757–762, 2001.

[15] D. L. Rudakov, J. A. Boedo, R. A. Moyer, S. Krasheninnikov, A. W. Leonard, M. A. Mahdavi, G. R. McKee, G. D. Porter, P. C. Stangeby, J. G. Watkins, W. P. West, D. G. Whyte, and G. Antar. Fluctuation-driven transport in the diii-d boundary. *Plasma Physics and Controlled Fusion*, 44(6):717–731, 2002.

[16] A. Kirk, T. Eich, A. Herrmann, H. W. Muller, L. D. Horton, G. F. Counsell, M. Price, V. Rohde, V. Bobkov, B. Kurzan, J. Neuhauser, and H. Wilson. The spatial structure of type-i elms at the mid-plane in asdex upgrade and a comparison with data from mast. *Plasma Physics and Controlled Fusion*, 47 (7):995–1013, 2005.

[17] A Kirk, N Ben Ayed, G Counsell, B Dudson, T Eich, A Herrmann, B Koch, R Martin, A Meakins, S Saarelma, R Scannell, S Tallents, M Walsh, H R Wilson, and the MAST team. Filament structures at the plasma edge on mast. *Plasma Physics and Controlled Fusion*, 48(12B):B433–B441, 2006. URL `http://stacks.iop.org/0741-3335/48/B433`.

[18] J. W. Connor. Edge-localized modes - physics and theory. *Plasma Physics and Controlled Fusion*, 40(5):531–542, 1998.

[19] H. R. Wilson and S. C. Cowley. Theory for explosive ideal magnetohydro-dynamic instabilities in plasmas. *Physical Review Letters*, 92(17):175006–1, 2004.

[20] P. Zhu, C. C. Hegna, C. R. Sovinec, A. Bhattacharjee, and K. Germaschewski. Intermediate nonlinear regime of a line-tied gmode. *Physics of Plasmas*, 14 (5), 2007.

[21] S. I. Krasheninnikov and A. I. Smolyakov. Generation of mesoscale convective structures in tokamak edge plasma. *Physics of Plasmas*, 14(10), 2007.

[22] R. Z. Sagdeev, V. D. Shapiro, and V. I. Shevchenko. Excitation of convective cells by alfven waves. *JETP Letters*, 27:340, 1978.

[23] R. Z. Sagdeev, V. D. Shapiro, and V. I. Shevchenko. Convective cells and anomalous plasma diffusion. *Soviet Journal of Plasma Physics*, 4(3):306–310, 1978.

[24] K. Mima and Y. C. Lee. Modulational instability of strongly dispersive drift waves and formation of convective cells. *Physics of Fluids*, 23(1):105–108, 1980.

[25] P. K. Shukla, M. Y. Yu, H. U. Rahman, and K. H. Spatschek. Excitation of convective cells by drift waves. *Physical Review A*, 23(1):321–324, Jan 1981. doi: 10.1103/PhysRevA.23.321.

[26] J. Weiland, H. Sanuki, and C. S. Liu. Convective cell formation and anomalous diffusion due to electromagnetic drift wave turbulence. *Physics of Fluids*, 24 (1):93–101, 1981.

[27] A. M. Balk, V. E. Zakharov, and S. V. Nazarenko. Nonlocal turbulence of drift waves. *Soviet Physics JETP*, 71:249, 1990.

[28] P. H. Diamond and Y. B. Kim. Theory of mean poloidal flow generation by turbulence. *Physics of Fluids B*, 3(7):1626–1633, 1991.

[29] Volker Naulin. Aspects of flow generation and saturation in drift-wave turbulence. *New Journal of Physics*, 4:28, 2002. URL `http://stacks.iop.org/1367-2630/4/28`.

[30] M G Shats and W M Solomon. Zonal flow generation in the improved confinement mode plasma and its role in confinement bifurcations. *New Journal of Physics*, 4:30, 2002. URL `http://stacks.iop.org/1367-2630/4/30`.

[31] F. Zonca, R. B. White, and L. Chen. Nonlinear paradigm for drift wave-zonal flow interplay: Coherence, chaos, and turbulence. *Physics of Plasmas*, 11 (5PART2):2488–2496, 2004.

[32] P. H. Diamond, S. I. Itoh, K. Itoh, and T. S. Hahm. Zonal flows in plasma - a review. *Plasma Physics and Controlled Fusion*, 47(5):R35–R161, 2005.

[33] K. Itoh, S. I. Itoh, P. H. Diamond, T. S. Hahm, A. Fujisawa, G. R. Tynan, M. Yagi, and Y. Nagashima. Physics of zonal flows. *Physics of Plasmas*, 13 (5), 2006.

[34] A. B. Mikhailovskii. *Theory of Plasma Instabilities*. New York, Consultants Bureau, 1974.

[35] M. N. Rosenbluth and A. Simon. Finite larmor radius equations with nonuniform electric fields and velocities. *Physics of Fluids*, 8(7):1300–1322, 1965.

[36] F. L. Hinton and C. W. Horton Jr. Amplitude limitation of a collisional drift wave instability. *Physics of Fluids*, 14(1):116–123, 1971.

[37] A. I. Smolyakov. Gyro viscous forces in a collision less plasma with temperature gradients. *Canadian Journal of Physics*, 76(4):321–331, 1998.

[38] O. Pogutse, W. Kerner, V. Gribkov, S. Bazdenkov, and M. Osipenko. The resistive interchange convection in the edge of tokamak plasmas. *Plasma Physics and Controlled Fusion*, 36(12):1963–1985, 1994. URL `http://stacks.iop.org/0741-3335/36/1963`.

[39] T. R. Bewley. *Numerical Renaissance: Simulation, Optimization and Control*. Renaissance Press, 2009. URL `http://numerical-renaissance.com/Numerical_Renaissance.html`.

[40] M. Endler. Turbulent sol transport in stellarators and tokamaks. *Journal of Nuclear Materials*, 266:84–90, 1999.

[41] E. Sanchez, C. Hidalgo, D. Lopez-Bruna, I. Garcia-Cortes, R. Balbin, M. A. Pedrosa, B. VanMilligen, C. Riccardi, G. Chiodini, J. Bleuel, M. Endler, B. A. Carreras, and D. E. Newman. Statistical characterization of fluctuation waveforms in the boundary region of fusion and non fusion plasmas. *Physics of Plasmas*, 7(5I):1408–1416, 2000.

[42] G. Y. Antar, S. I. Krasheninnikov, P. Devynck, R. P. Doerner, E. M. Hollmann, J. A. Boedo, S. C. Luckhardt, and R. W. Conn. Experimental evidence of intermittent convection in the edge of magnetic confinement devices. *Physical Review Letters*, 87(6):650011–650014, 2001.

[43] Th. Pierre, A. Escarguel, D. Guyomarc'h, R. Barni, and C. Riccardi. Radial convection of plasma structures in a turbulent rotating magnetized-plasma column. *Physical Review Letters*, 92(6):650041–650044, 2004.

[44] T. A. Carter. Intermittent turbulence and turbulent structures in a linear magnetized plasma. *Physics of Plasmas*, 13(1):1–4, 2006.

[45] S. I. Krasheninnikov and A. I. Smolyakov. On neutral wind and blob motion in linear devices. *Physics of Plasmas*, 10(7):3020–3021, 2003.

[46] S. I. Krasheninnikov, A. I. Smolyakov, and T. K. Soboleva. On anomalous cross-field edge plasma convection in fusion devices. *Physics of Plasmas*, 12 (7):072502, 2005. doi: 10.1063/1.1940061.

[47] I. Eames and J. C. R. Hunt. Inviscid flow around bodies moving in weak density gradients without buoyancy effects. *Journal of Fluid Mechanics*, 353: 331–355, 1997.

[48] G. K. Batchelor. *An Introduction to Fluid Dynamics*. Cambridge, University Press, 1967.

[49] W. H. Wang, Y. X. He, Z. Gao, L. Zeng, G. P. Zhang, L. F. Xie, X. Z. Yang, C. H. Feng, L. Wang, Q. Xiao, and X. Y. Li. Edge plasma electrostatic fluctuation and anomalous transport characteristics in the sino-united spherical tokamak. *Plasma Physics and Controlled Fusion*, 47(1):1–16, 2005.

[50] A. K. Singh, J. Morelli, T. Asai, and A. Hirose. Observation of radial propagation of electrostatic fluctuations in the saskatchewan torus-modified tokamak. *Physics of Plasmas*, 10(9):3451–3454, 2003.

[51] N. Mattor and P. H. Diamond. Drift wave propagation as a source of plasma edge turbulence. *Physical Review Letters*, 72(4):486–489, 1994.

[52] A. J. Wootton, B. A. Carreras, H. Matsumoto, K. McGuire, W. A. Peebles, Ch. P. Ritz, P. W. Terry, and S. J. Zweben. Fluctuations and anomalous transport in tokamaks. *Physics of Fluids B: Plasma Physics*, 2(12):2879–2903, 1990. doi: 10.1063/1.859358.

[53] A. J. Brizard and T. S. Hahm. Foundations of nonlinear gyrokinetic theory. *Reviews of Modern Physics*, 79(2):421–468, 2007.

[54] P. L. Bhatnagar, E. P. Gross, and M. Krook. A model for collision processes in gases. i. small amplitude processes in charged and neutral one-component systems. *Physical Review*, 94(3):511–525, May 1954. doi: 10.1103/PhysRev.94.511.